Jet Formation and Propagation in FSRQs and BL Lacs

Will Potter
Junior Research Fellow,
University College, University of Oxford

Talk Structure

- Introduction to blazars - FSRQs and BL Lacs.
- A realistic extended fluid jet emission model.
- Constraining the structure and dynamics of jets.
- How the physical properties of blazar jets influence their spectra and classification.
- How FSRQs and BL Lacs relate to AGN unification and the accretion mode dichotomy.

Blazars – what are FSRQs and BL Lacs?

- Blazars are AGN with jets directed close to the Earth.
- The relativistic jet speeds mean that the emission from the jets is highly Doppler boosted.
- This makes blazars excellent objects to understand jet properties since the jet emission outshines the galactic and disc emission.
- Blazars are classified by the width of the optical emission lines.
- FSRQ – Flat Spectrum Radio Quasar. Emission lines widths are greater than 5Å.
- BL Lacs – named after BL Lacertae (which is amusingly sometimes a BL Lac and sometimes not). Emission line widths smaller than 5Å.

Blazar spectra

- Blazar spectra are characterised by two bumps, well fitted by synchrotron and inverse-Compton emission of high-energy electrons.

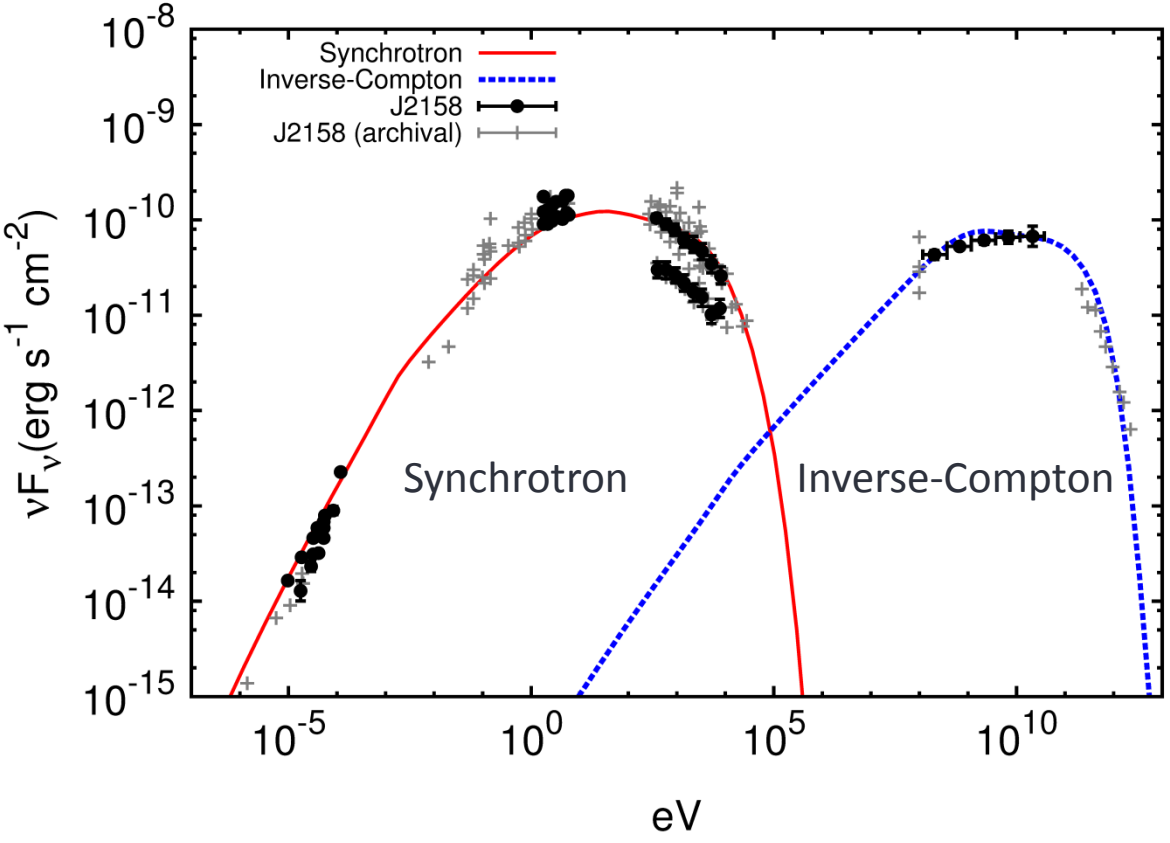

What are the differences between FSRQs and BL Lacs? – The blazar sequence

- As you increase the radio luminosity blazars have lower peak frequencies of emission and become more Compton-dominant.
- High power blazars are mostly FSRQs and low power blazars are mostly BL Lacs.

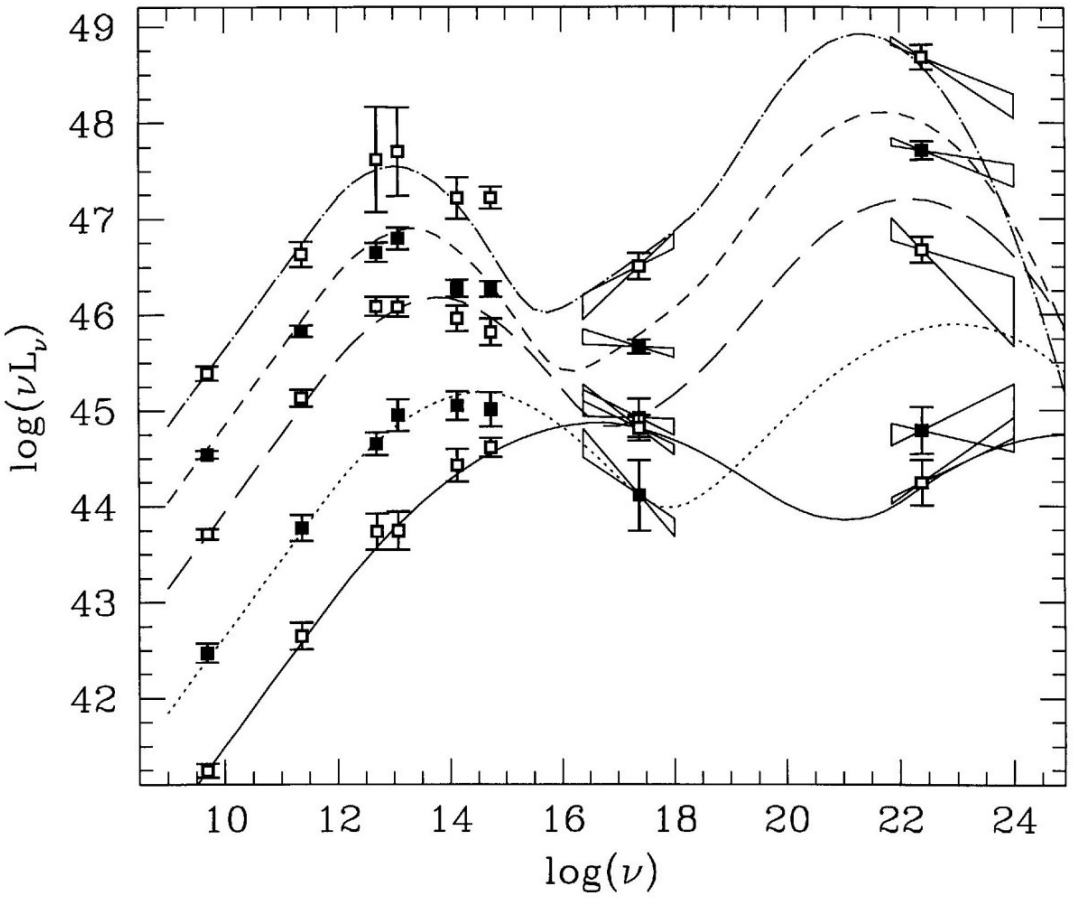

Fossati et al. 1998

Jet simulations

- General relativistic MHD simulations find jets which start magnetically dominated and parabolic in the accelerating region.
- Once the jets have accelerated and converted most of the magnetic energy to bulk kinetic energy the acceleration ceases to be efficient (at ~1000 Schwarzschild radii) and the jets become ballistic and conical.

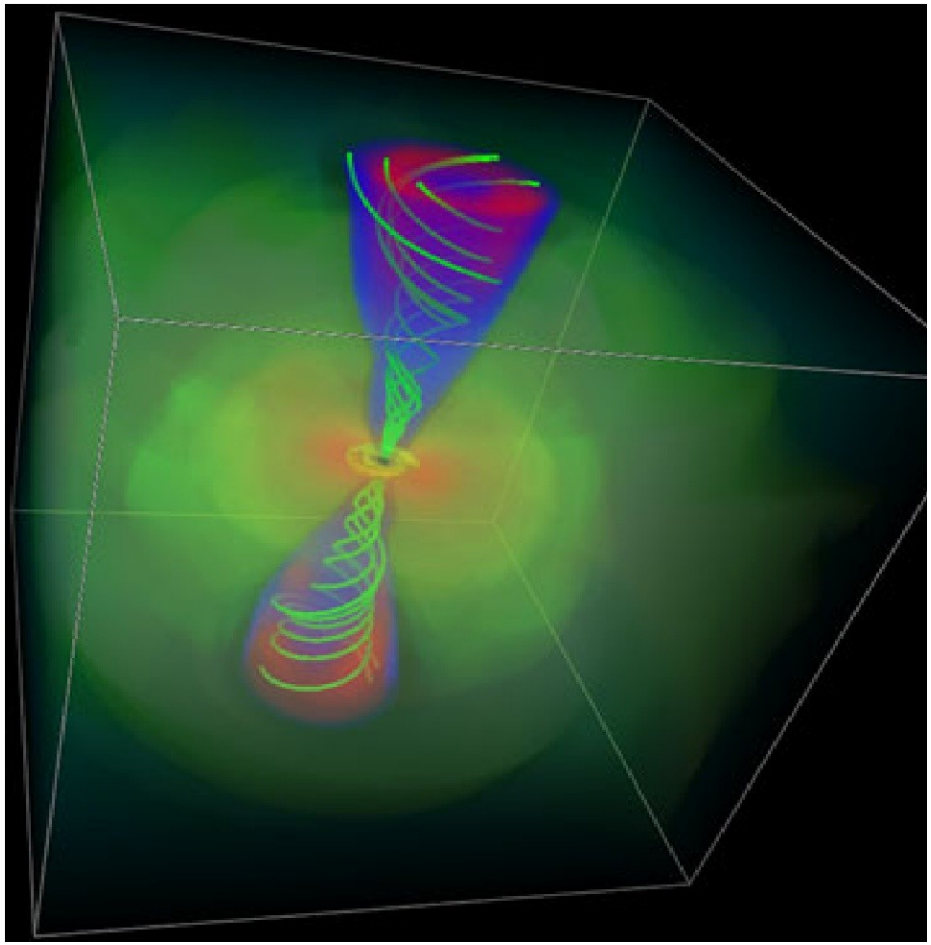

McKinney and Blandford 2009

Observations of jets

- The nearest jet M87 has been observed with radio VLBI and the shape has been found to start parabolic and transition to conical at 10^5 r_s.

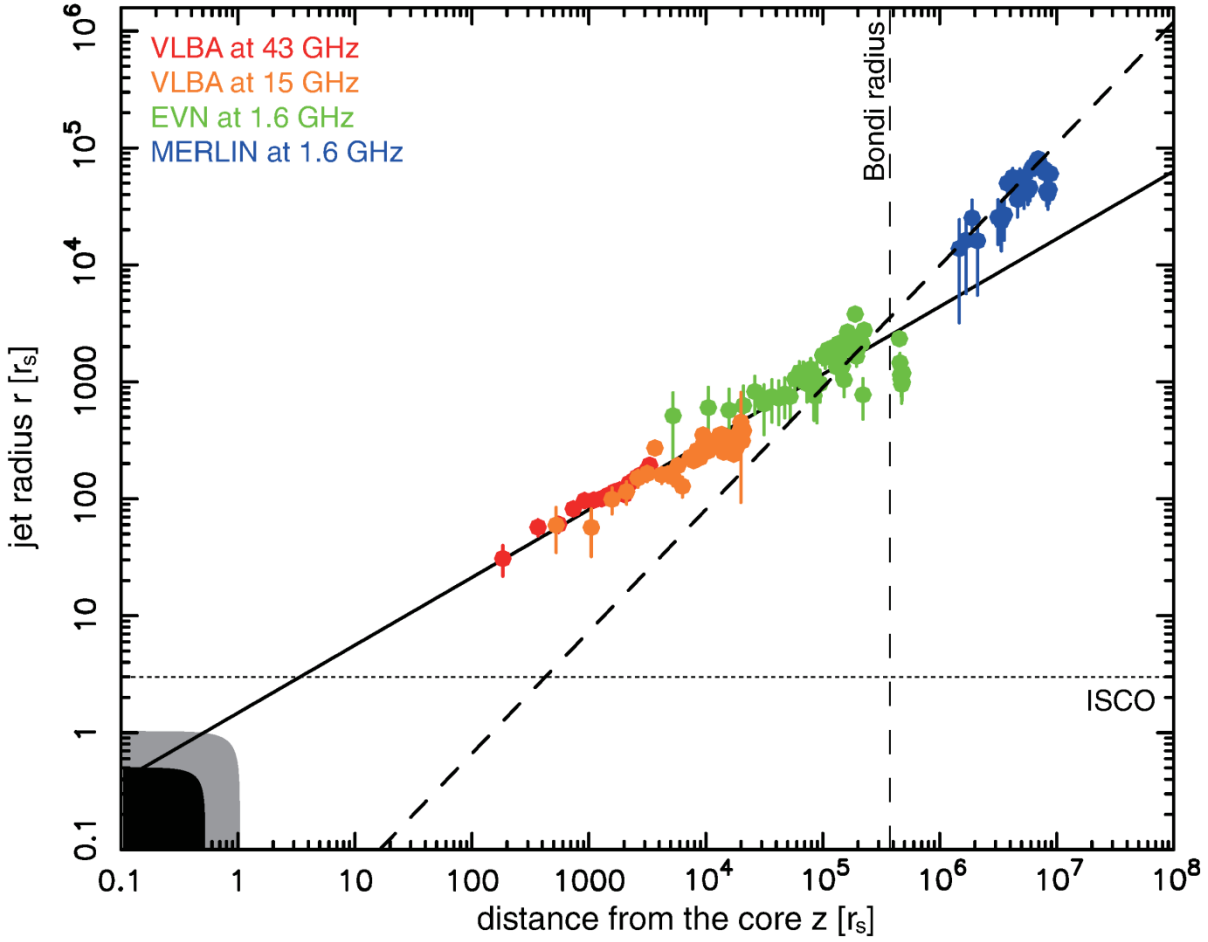

Asada and Nakamura 2011

Why model blazar emission?

- There seems to be a reasonable consistency between observations, simulations and theory.
- The information we posses on real jets comes from observing the radiation they emit.
- It is too computationally expensive to include a detailed calculation of the emission in GRMHD simulations .
- We need jet emission models which are able to constrain the jet properties and predictions from simulations by comparing to observed spectra.
- Blazars are the optimal sources to model since essentially all the emission is from the jet.

Comparison to existing models

- Existing spherical blob and cylindrical jet emission models are successful at high frequencies but cannot reproduce the observed radio emission produced by the large scale structure of the jet.

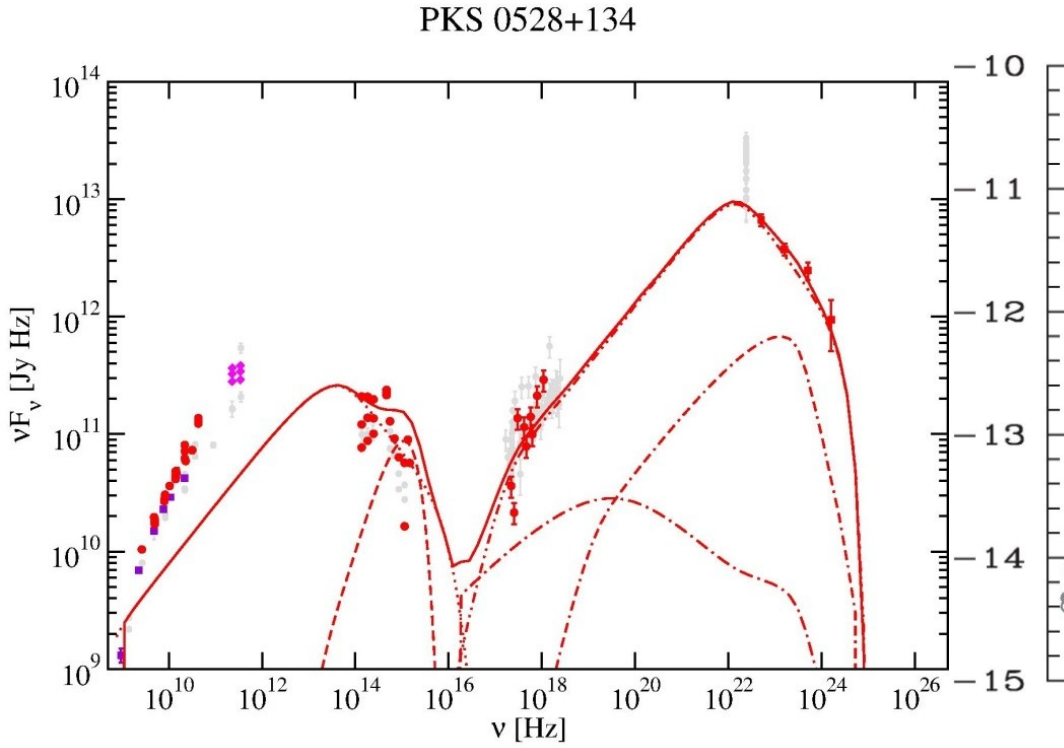

Bottcher et al. 2013

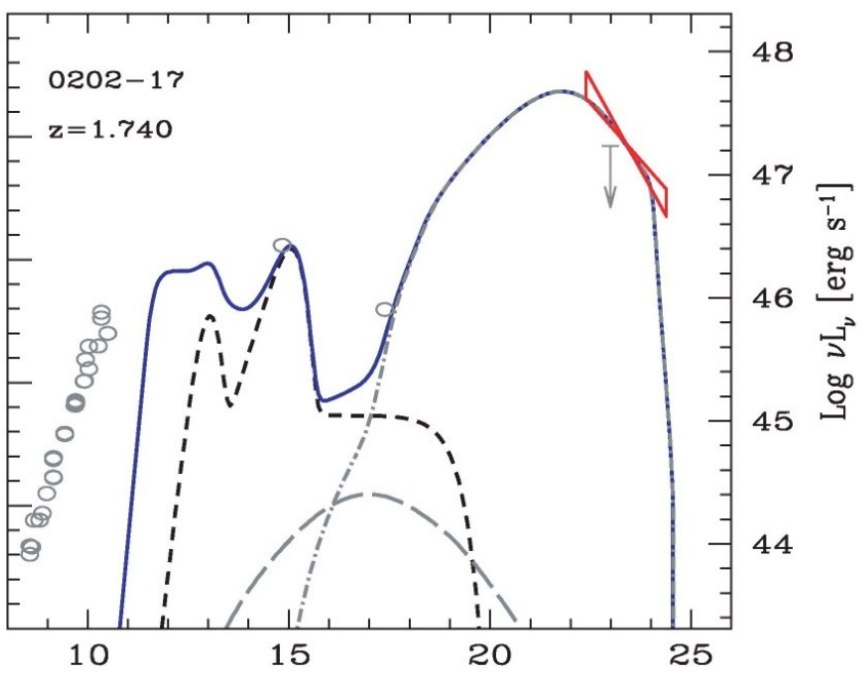

Ghisellini et al. 2009

A realistic, extended model for jet emission

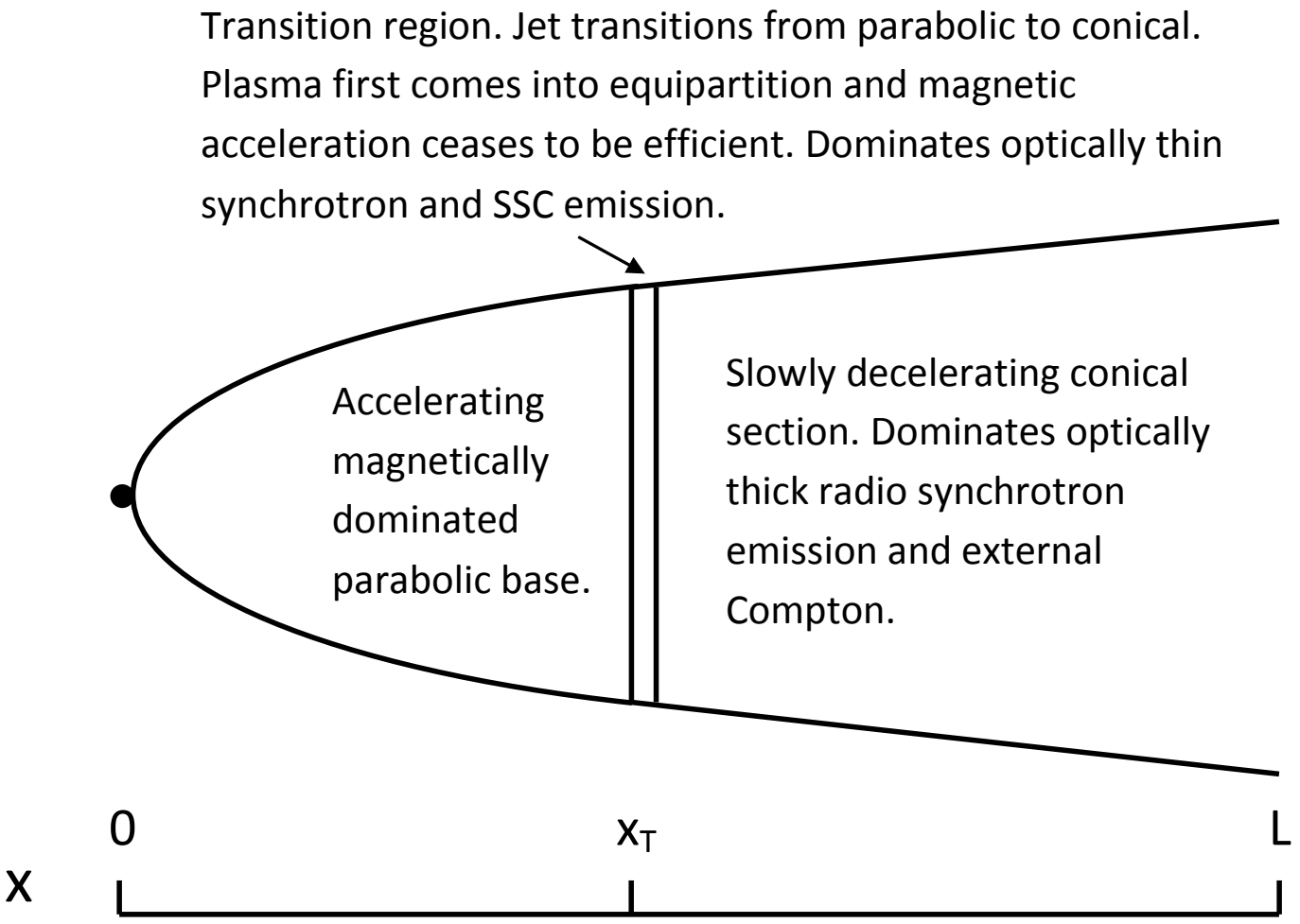

Potter and Cotter 2015

A fluid jet model – conservation of energy

- We assume jet properties only depend on the jet length and are homogeneous perpendicular to the jet axis.
- Since we allow the jet velocity and shape to change as a function of distance conservation of relativistic energy-momentum takes the form.

$$\nabla_\mu T^{\mu\nu} = 0, \qquad T^{\mu\nu} = T^{\mu\nu}_{\text{Magnetic}} + T^{\mu\nu}_{\text{Particles}} + T^{\mu\nu}_{\text{Losses}}$$

- In order to relate plasma properties in the rest frame and lab frame we treat the plasma as a relativistic perfect fluid.

$$T'^{\mu\nu} = \begin{pmatrix} \rho' & 0 & 0 & 0 \\ 0 & \frac{\rho'}{3} & 0 & 0 \\ 0 & 0 & \frac{\rho'}{3} & 0 \\ 0 & 0 & 0 & \frac{\rho'}{3} \end{pmatrix} \qquad T^{\mu\nu}(x) = \Lambda^{\mu}{}_{\text{a}} T'^{\text{ab}} \Lambda^{\nu}{}_{\text{b}} = \begin{pmatrix} \frac{4}{3}\gamma_{\text{bulk}}(x)^2\rho' & \frac{4}{3}\gamma_{\text{bulk}}(x)^2\rho' & 0 & 0 \\ \frac{4}{3}\gamma_{\text{bulk}}(x)^2\rho' & \frac{4}{3}\gamma_{\text{bulk}}(x)^2\rho' & 0 & 0 \\ 0 & 0 & \frac{\rho'}{3} & 0 \\ 0 & 0 & 0 & \frac{\rho'}{3} \end{pmatrix}$$

- Integrating conservation of energy over the jet volume and using the divergence theorem we find the conservation of energy equation for the jet.

$$\int \nabla_\mu T^{\mu\nu} \mathrm{d}^4 V = \int T^{\mu\nu} \mathrm{d}^3 S^\mu = \frac{\partial}{\partial x}\left(\frac{4}{3}\gamma_{\text{bulk}}(x)^2 \pi R^2(x) \rho'(x)\right) = 0$$

Calculating the synchrotron and inverse-Compton emission

- Divide the jet into thousands of cylindrical sections to match the extended structure and bulk Lorentz factors.
- Calculate the synchrotron and inverse-Compton emission from the non-thermal electrons in each section as the plasma propagates along the jet.
- Integrate the synchrotron and pair-production opacity to a section and sum the emission from all sections.
- Take into account radiative and adiabatic energy losses to the electron population and reacceleration processes.
- Include a detailed treatment of all relevant external photon sources: accretion disc, BLR, dusty torus, NLR, starlight and CMB.

External photon fields

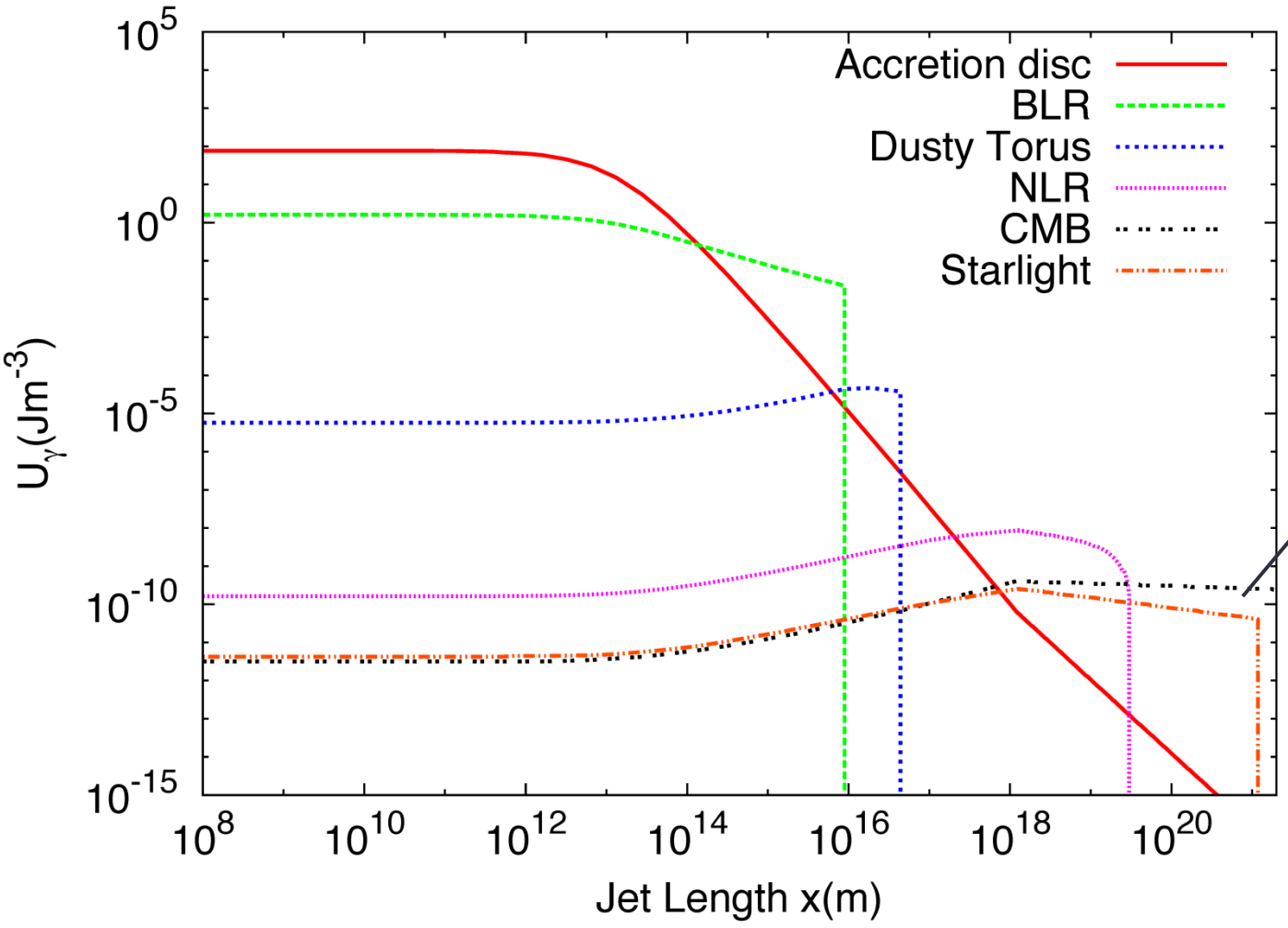

CMB dominates at large distances

Potter and Cotter 2015

Fitting the model to spectra

- For the first time the model fits to both radio and gamma-ray blazar observations simultaneously.

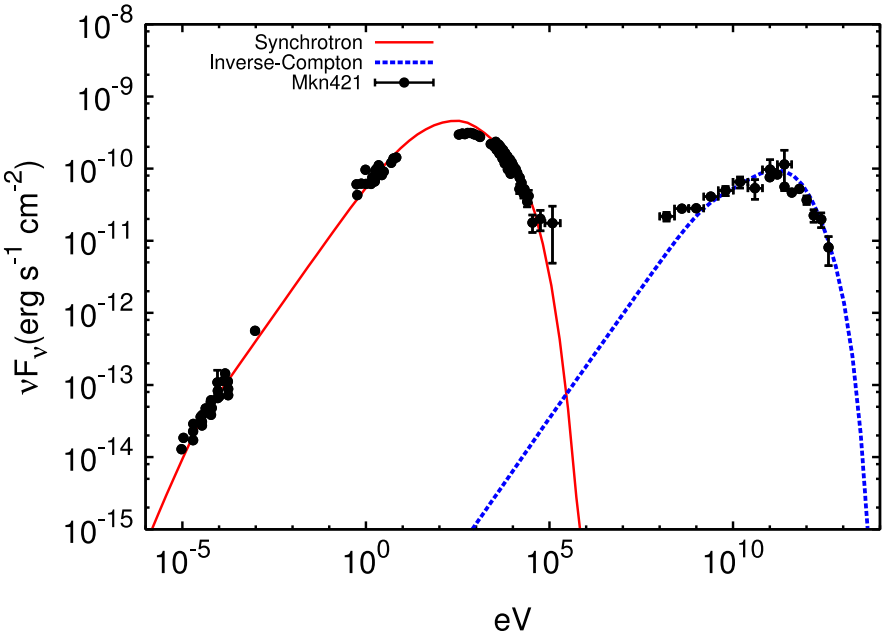

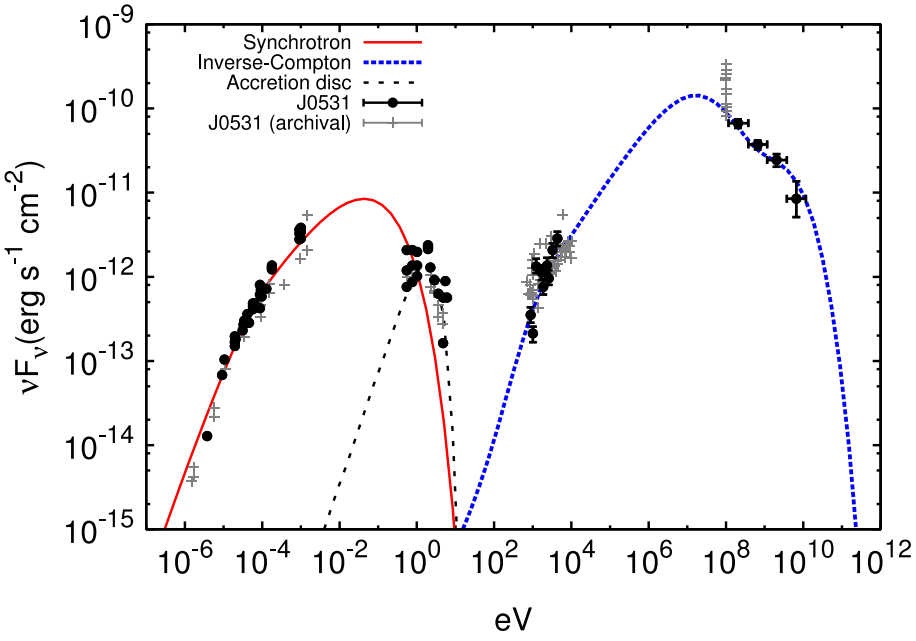

Potter and Cotter 2013b, 2013c and 2015

Fitting to 38 simultaneous multiwavelength Fermi blazars

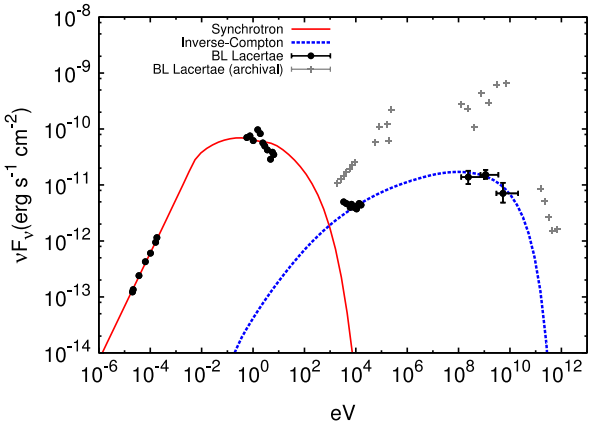

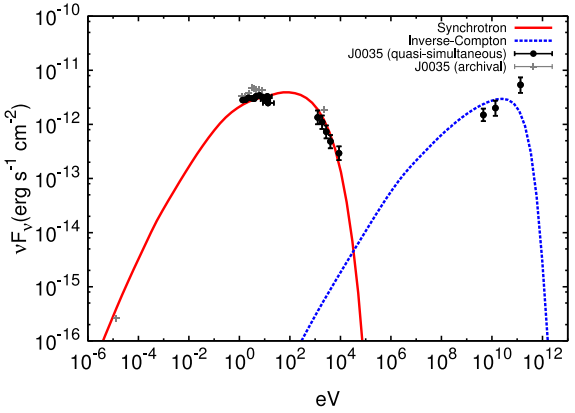

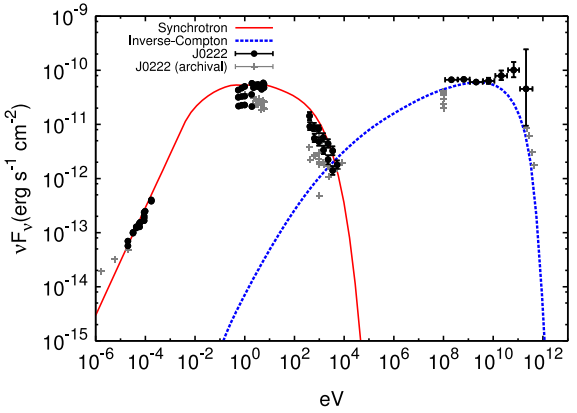

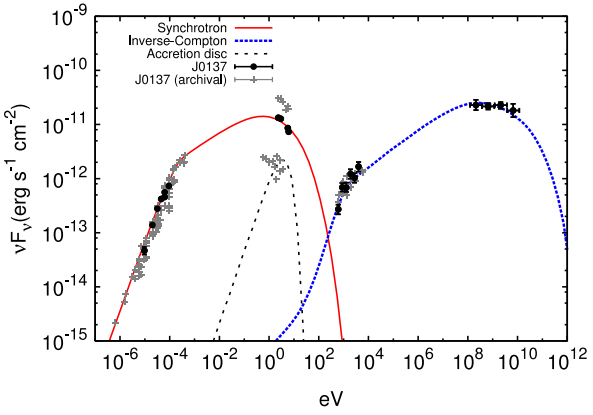

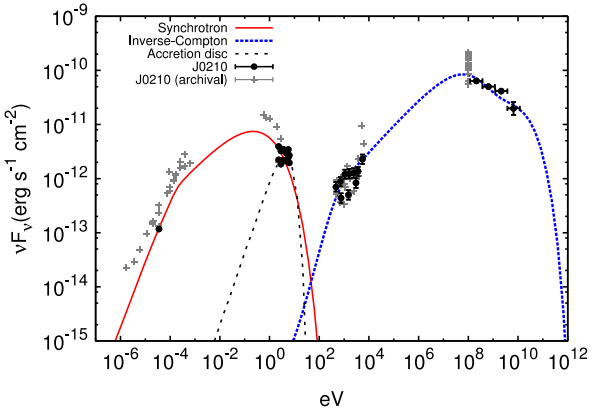

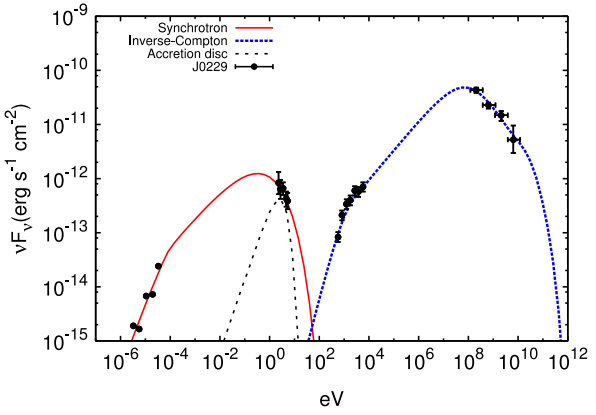

Potter and Cotter 2013b, 2013c and 2015

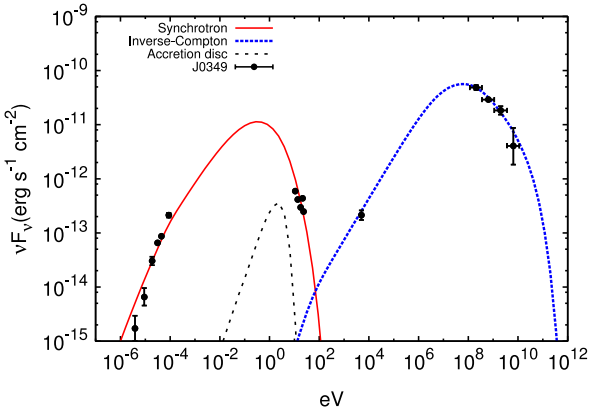
Synchrotron
Inverse-Compton
Accretion disc
J0349
νF_ν(erg s^{-1} cm^{-2})
eV

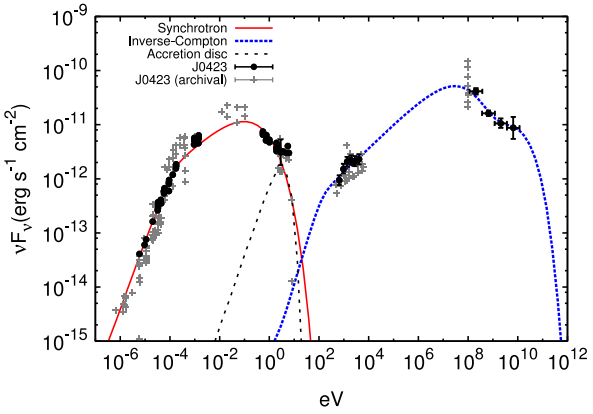
Synchrotron
Inverse-Compton
Accretion disc
J0423
J0423 (archival)
νF_ν(erg s^{-1} cm^{-2})
eV

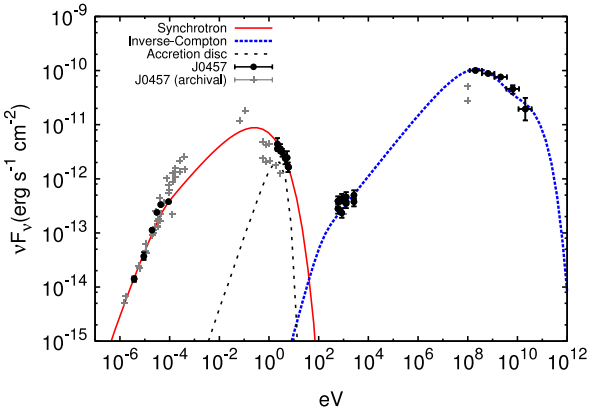
Synchrotron
Inverse-Compton
Accretion disc
J0457
J0457 (archival)
νF_ν(erg s^{-1} cm^{-2})
eV

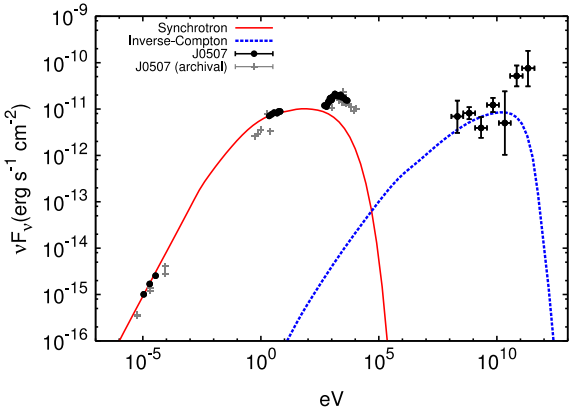
Synchrotron
Inverse-Compton
J0507
J0507 (archival)
νF_ν(erg s^{-1} cm^{-2})
eV

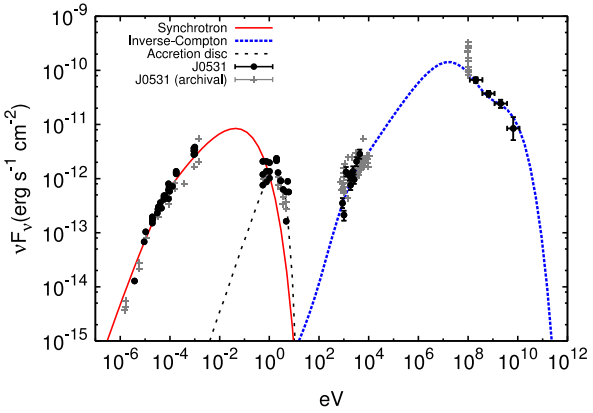
Synchrotron
Inverse-Compton
Accretion disc
J0531
J0531 (archival)
νF_ν(erg s^{-1} cm^{-2})
eV

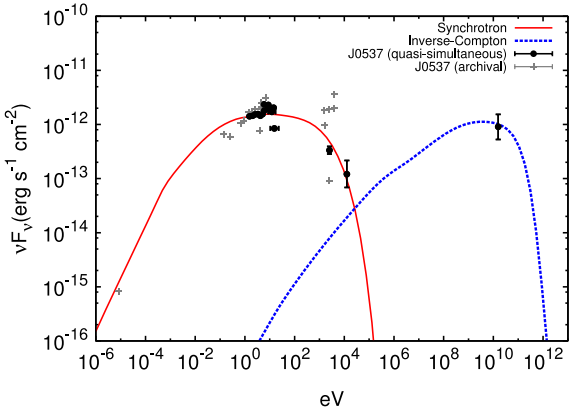
Synchrotron
Inverse-Compton
J0537 (quasi-simultaneous)
J0537 (archival)
νF_ν(erg s^{-1} cm^{-2})
eV

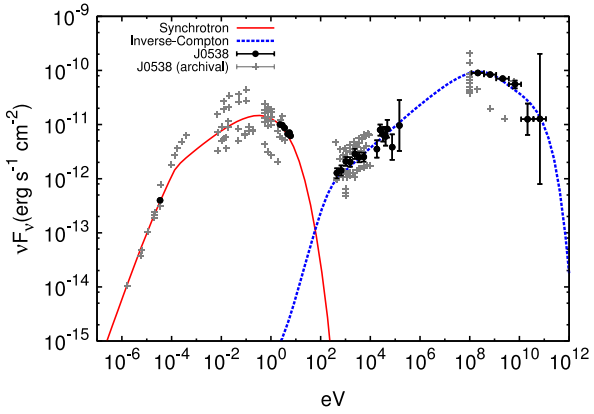
Synchrotron
Inverse-Compton
J0538
J0538 (archival)
νF_ν(erg s^{-1} cm^{-2})
eV

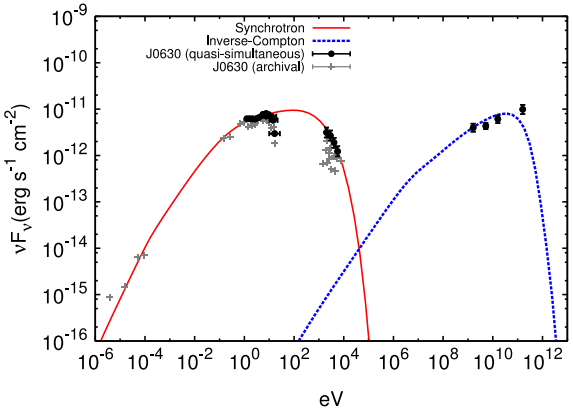
Synchrotron
Inverse-Compton
J0630 (quasi-simultaneous)
J0630 (archival)
νF_ν(erg s^{-1} cm^{-2})
eV

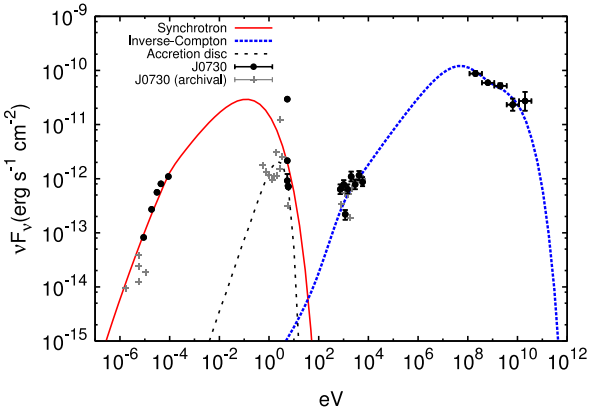
Synchrotron
Inverse-Compton
Accretion disc
J0730
J0730 (archival)
νF_ν(erg s^{-1} cm^{-2})
eV

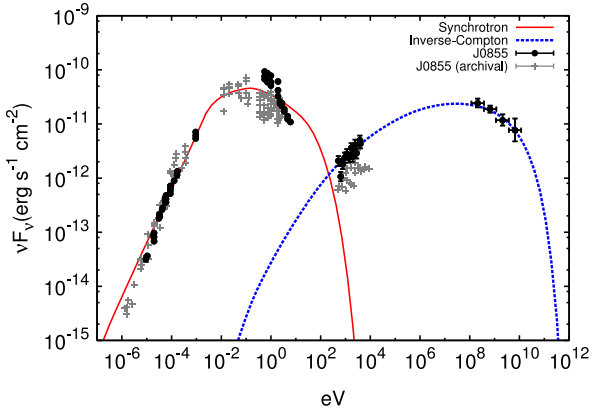
Synchrotron
Inverse-Compton
J0855
J0855 (archival)
νF_ν(erg s^{-1} cm^{-2})
eV

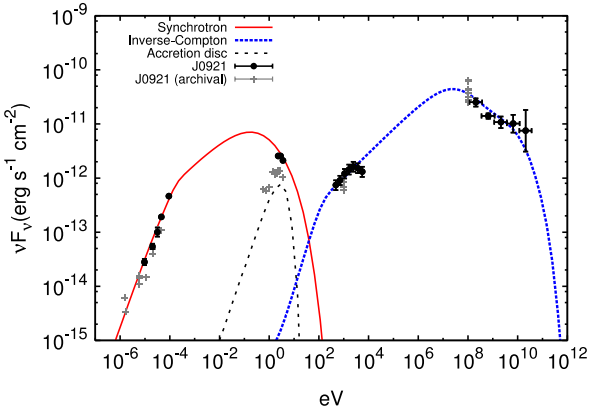
Synchrotron
Inverse-Compton
Accretion disc
J0921
J0921 (archival)
νF_ν(erg s^{-1} cm^{-2})
eV

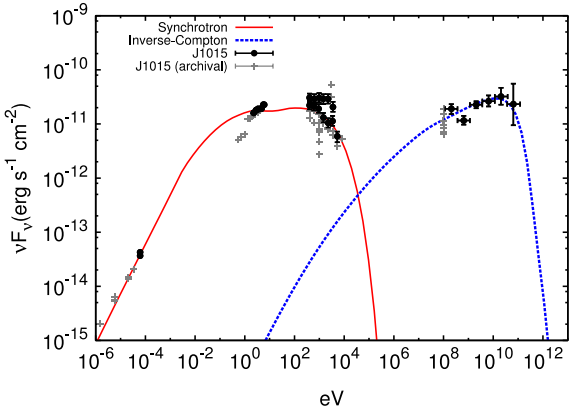
Synchrotron
Inverse-Compton
J1015
J1015 (archival)
νF_ν(erg s^{-1} cm^{-2})
eV

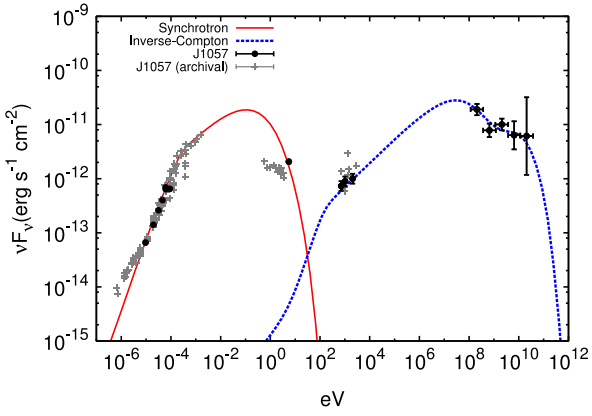
Synchrotron
Inverse-Compton
J1057
J1057 (archival)
νF_ν(erg s^{-1} cm^{-2})
eV

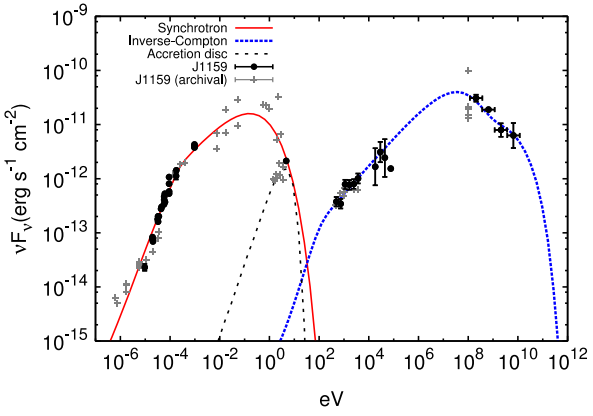
Synchrotron
Inverse-Compton
Accretion disc
J1159
J1159 (archival)
νF_ν(erg s^{-1} cm^{-2})
eV

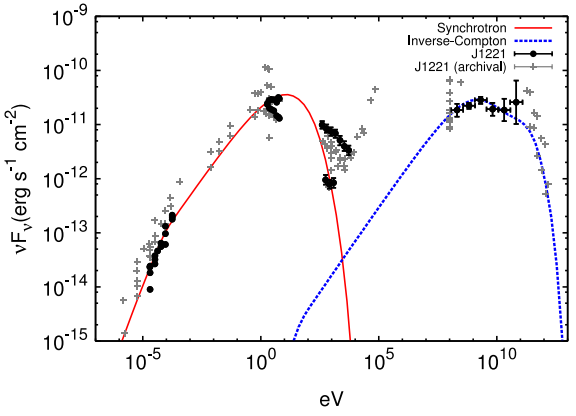
Synchrotron
Inverse-Compton
J1221
J1221 (archival)
νF_ν(erg s^{-1} cm^{-2})
eV

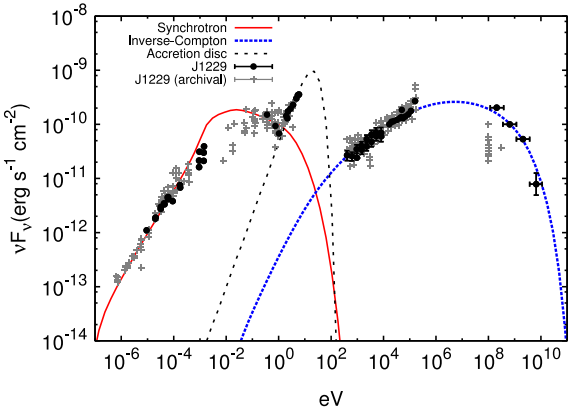
Synchrotron
Inverse-Compton
Accretion disc
J1229
J1229 (archival)
νF_ν(erg s^{-1} cm^{-2})
eV

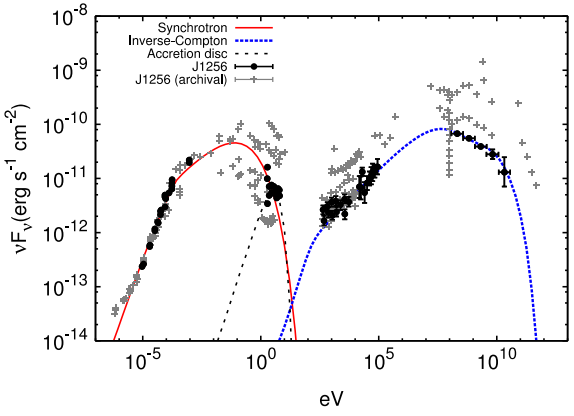
Synchrotron
Inverse-Compton
Accretion disc
J1256
J1256 (archival)
νF_ν(erg s^{-1} cm^{-2})
eV

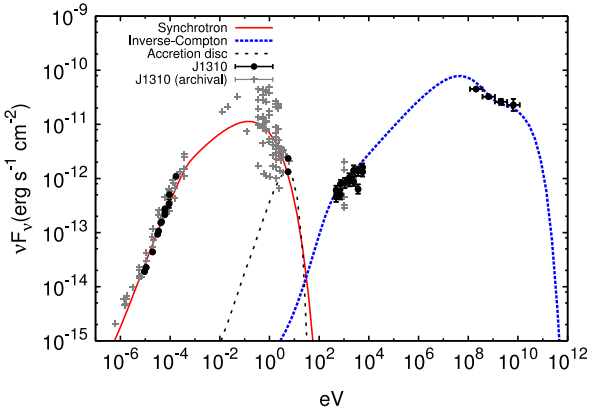
Synchrotron
Inverse-Compton
Accretion disc
J1310
J1310 (archival)
νF_ν(erg s^{-1} cm^{-2})
eV

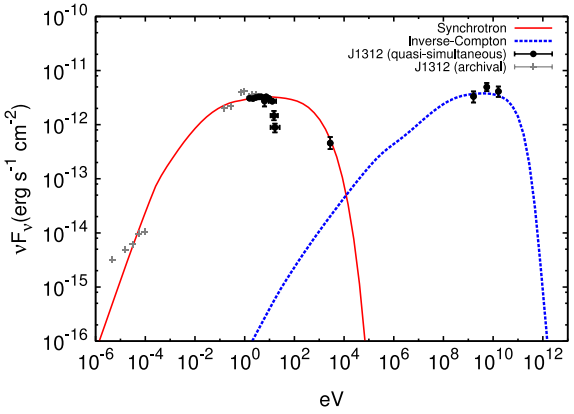
Synchrotron
Inverse-Compton
J1312 (quasi-simultaneous)
J1312 (archival)
νF_ν(erg s^-1 cm^-2)
eV

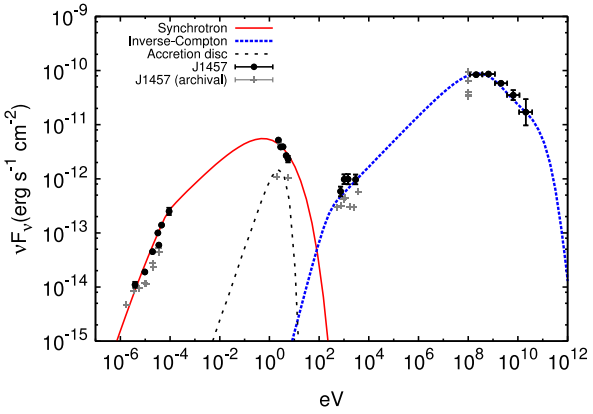
Synchrotron
Inverse-Compton
Accretion disc
J1457
J1457 (archival)
νF_ν(erg s^-1 cm^-2)
eV

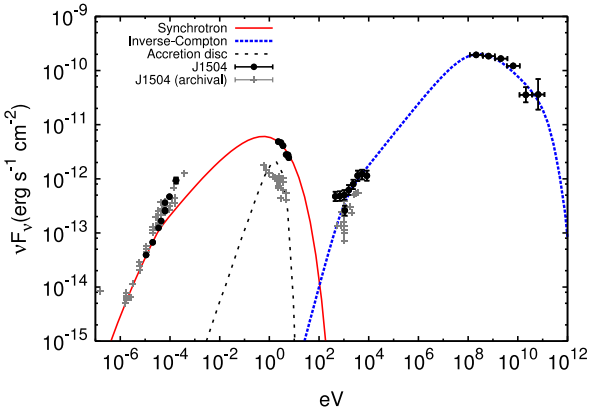
Synchrotron
Inverse-Compton
Accretion disc
J1504
J1504 (archival)
νF_ν(erg s^-1 cm^-2)
eV

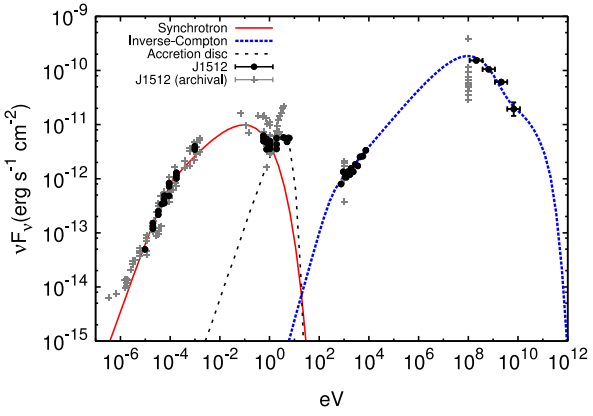
Synchrotron
Inverse-Compton
Accretion disc
J1512
J1512 (archival)
νF_ν(erg s^-1 cm^-2)
eV

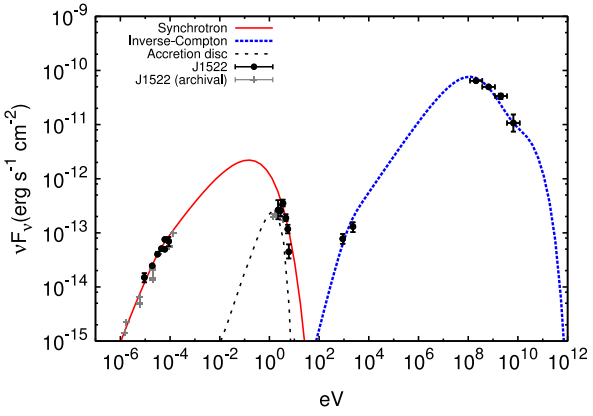
Synchrotron
Inverse-Compton
Accretion disc
J1522
J1522 (archival)
νF_ν(erg s^-1 cm^-2)
eV

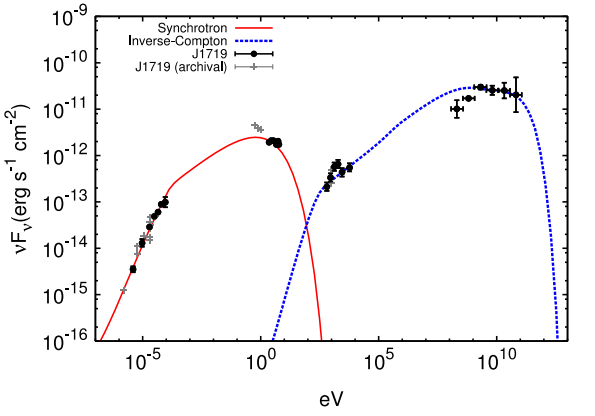
Synchrotron
Inverse-Compton
J1719
J1719 (archival)
νF_ν(erg s^-1 cm^-2)
eV

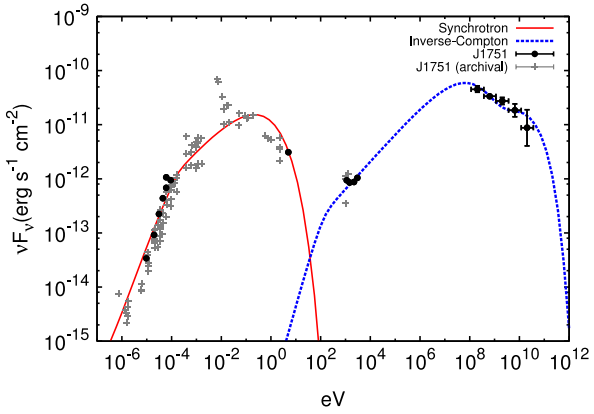
Synchrotron
Inverse-Compton
J1751
J1751 (archival)
νF_ν(erg s^{-1} cm^{-2})
eV

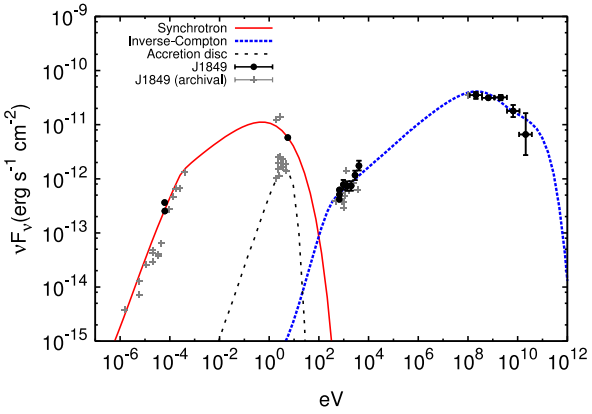
Synchrotron
Inverse-Compton
Accretion disc
J1849
J1849 (archival)
νF_ν(erg s^{-1} cm^{-2})
eV

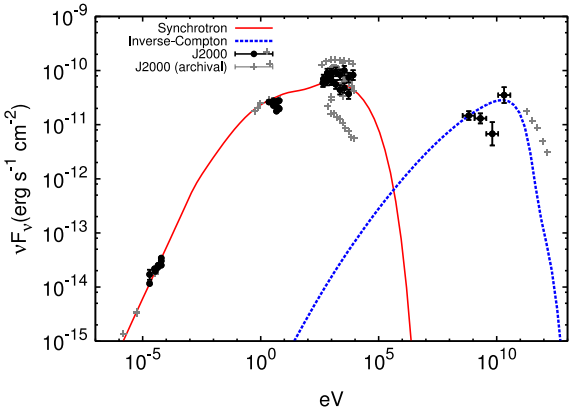
Synchrotron
Inverse-Compton
J2000
J2000 (archival)
νF_ν(erg s^{-1} cm^{-2})
eV

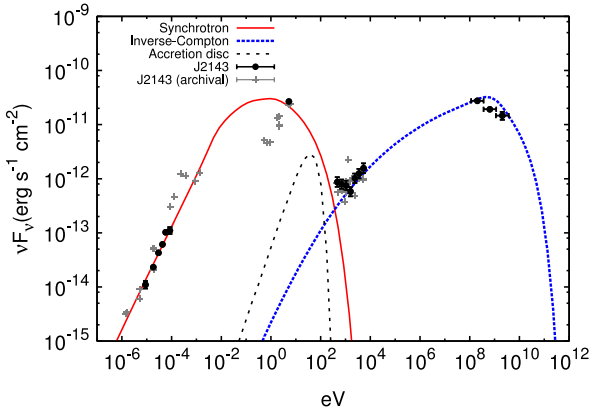
Synchrotron
Inverse-Compton
Accretion disc
J2143
J2143 (archival)
νF_ν(erg s^{-1} cm^{-2})
eV

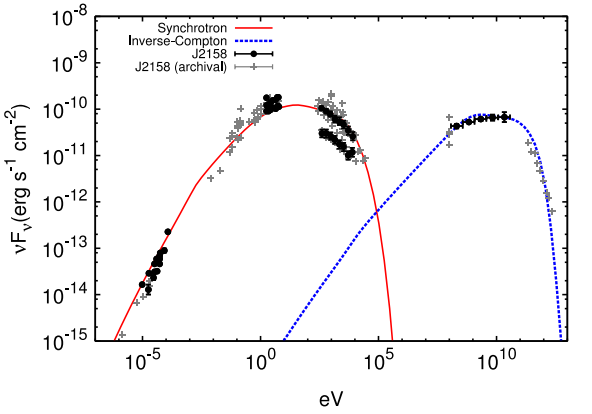
Synchrotron
Inverse-Compton
J2158
J2158 (archival)
νF_ν(erg s^{-1} cm^{-2})
eV

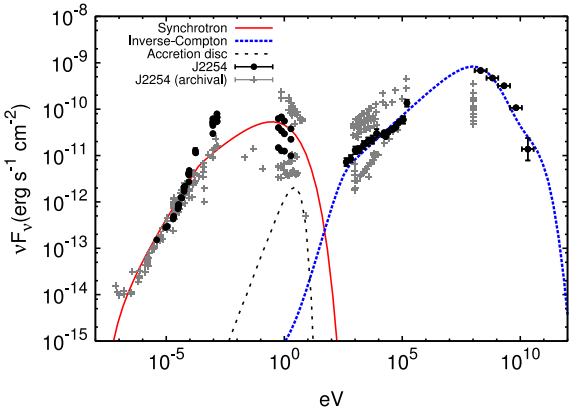
Synchrotron
Inverse-Compton
Accretion disc
J2254
J2254 (archival)
νF_ν(erg s^{-1} cm^{-2})
eV

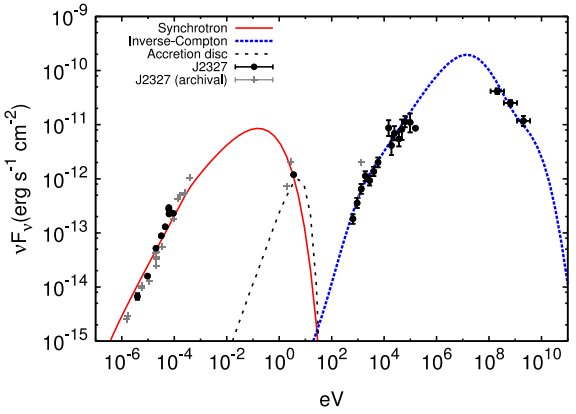
Synchrotron
Inverse-Compton
Accretion disc
J2327
J2327 (archival)
νF_ν(erg s^{-1} cm^{-2})
eV

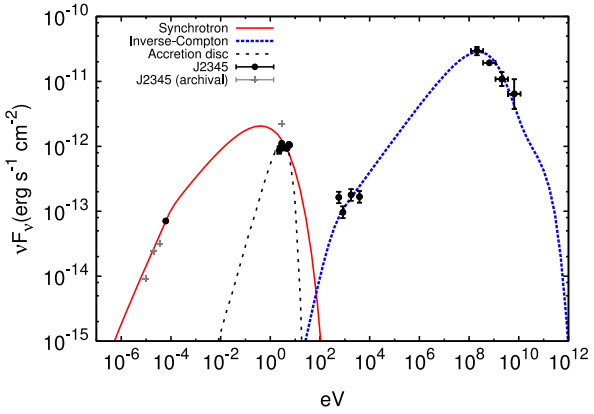
Synchrotron
Inverse-Compton
Accretion disc
J2345
J2345 (archival)
νF_ν(erg s^{-1} cm^{-2})
eV

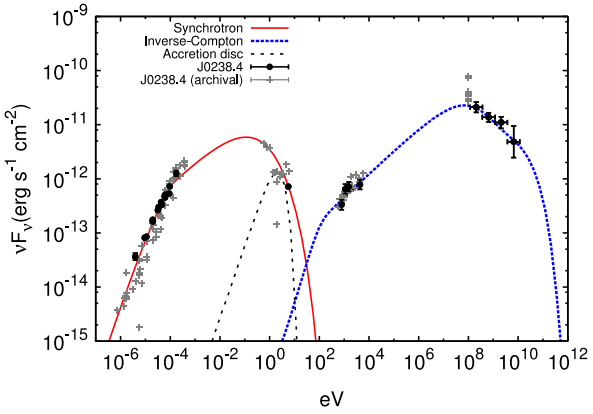
Synchrotron
Inverse-Compton
Accretion disc
J0238.4
J0238.4 (archival)
νF_ν(erg s^{-1} cm^{-2})
eV

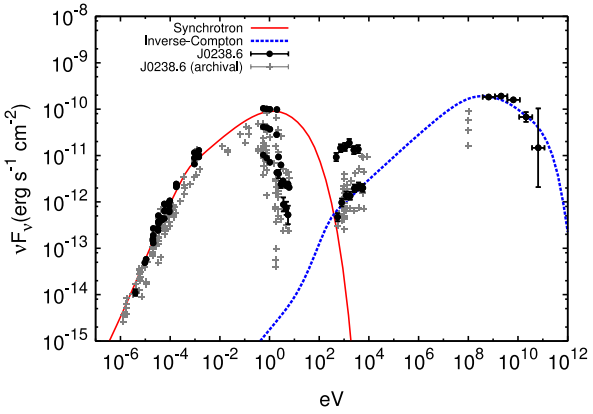
Synchrotron
Inverse-Compton
J0238.6
J0238.6 (archival)
νF_ν(erg s^{-1} cm^{-2})
eV

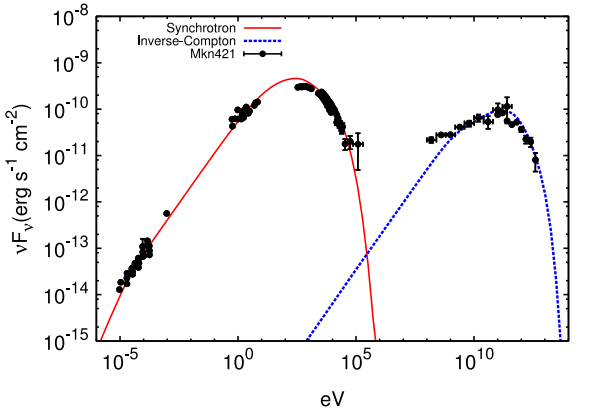
Synchrotron
Inverse-Compton
Mkn421
νF_ν(erg s^{-1} cm^{-2})
eV

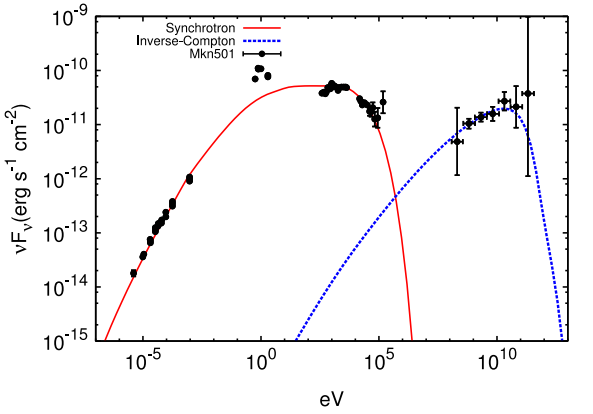
Synchrotron
Inverse-Compton
Mkn501
νF_ν(erg s^{-1} cm^{-2})
eV

Constraining the radius of the transition region

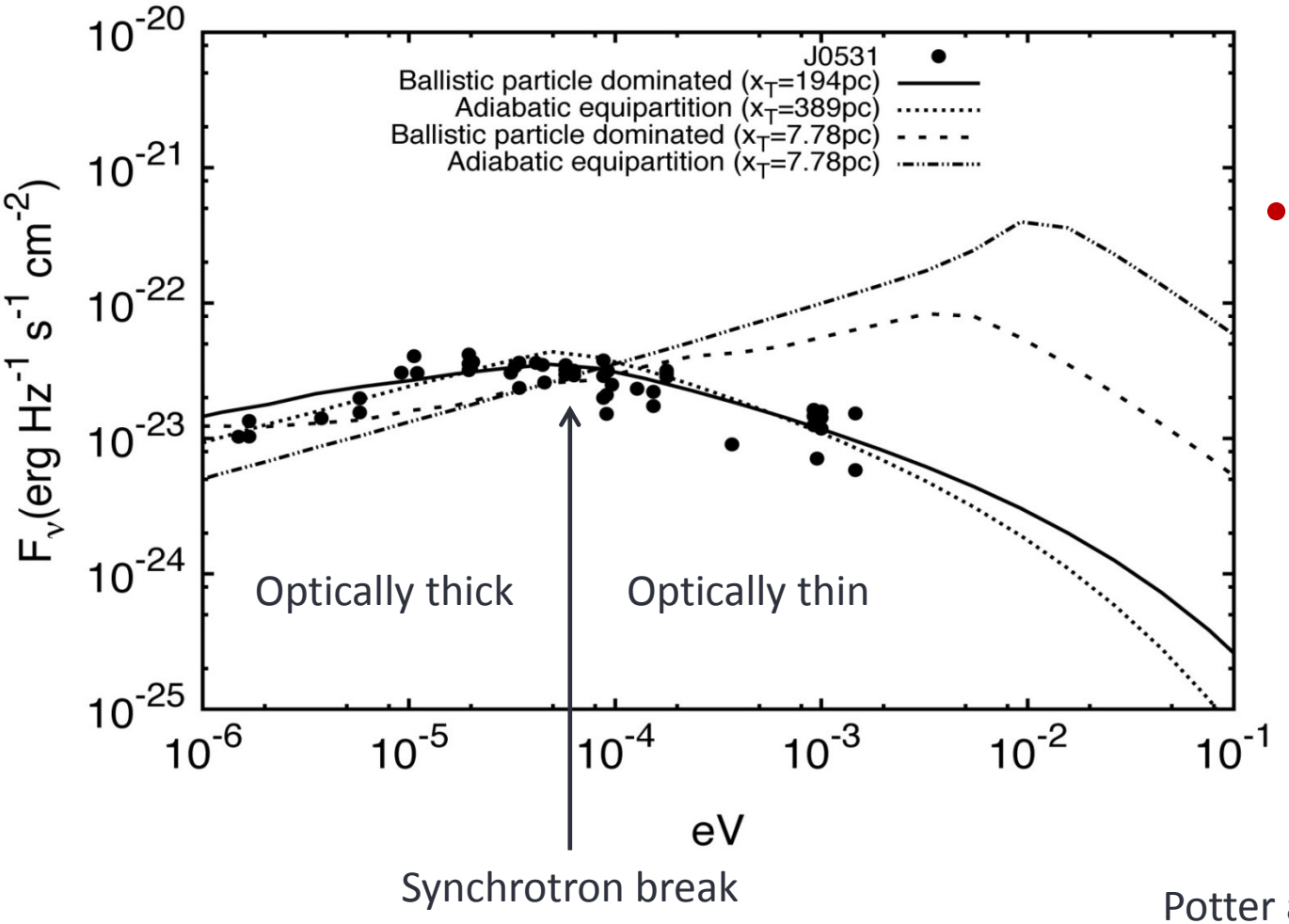

- In M87:
  $R_T=2000r_s$
  $x_T=10^5r_s$

Potter and Cotter 2013b

An approximately linear correlation between jet power and transition region radius!

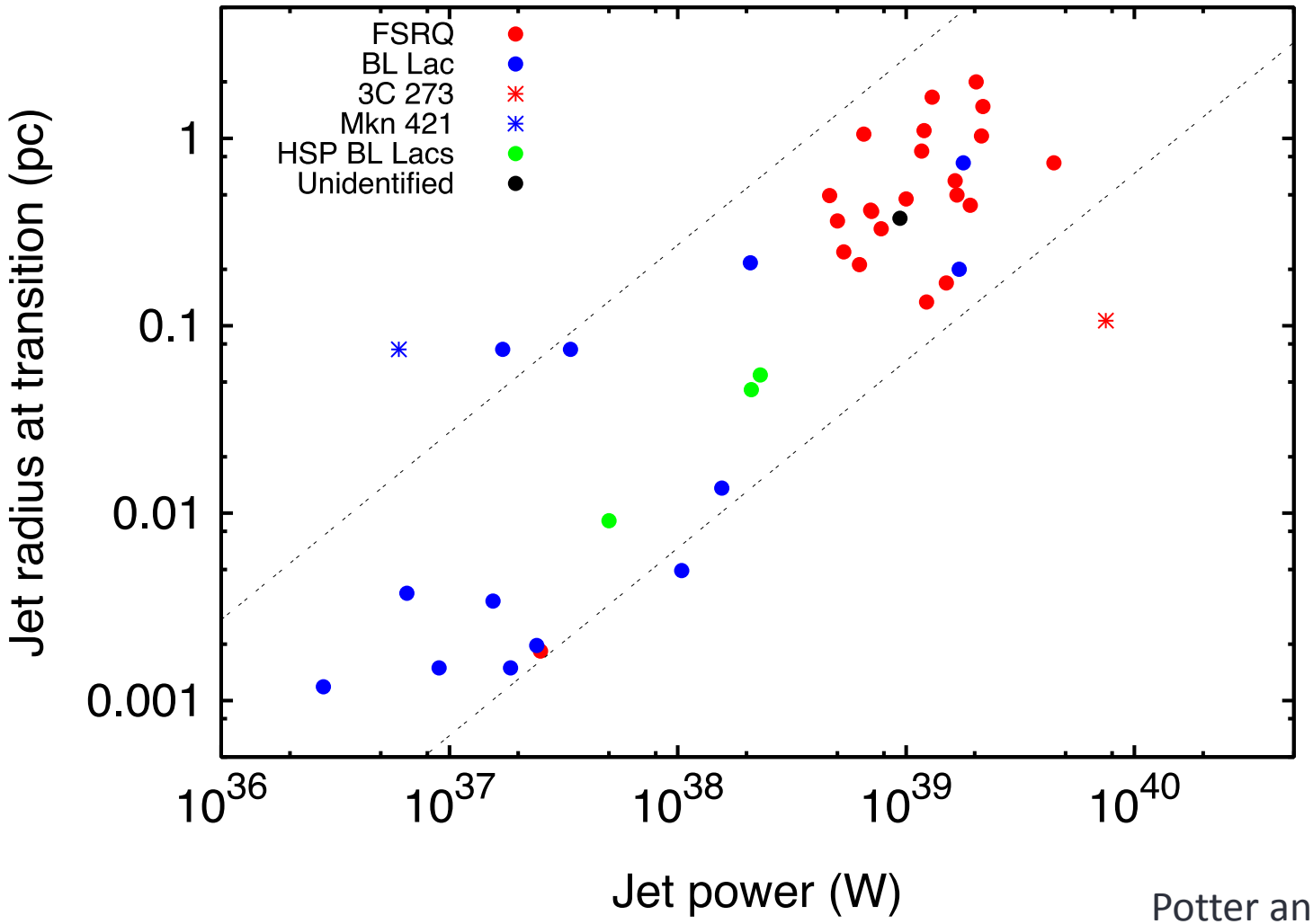

Potter and Cotter 2015

Jet power vs. bulk Lorentz factor

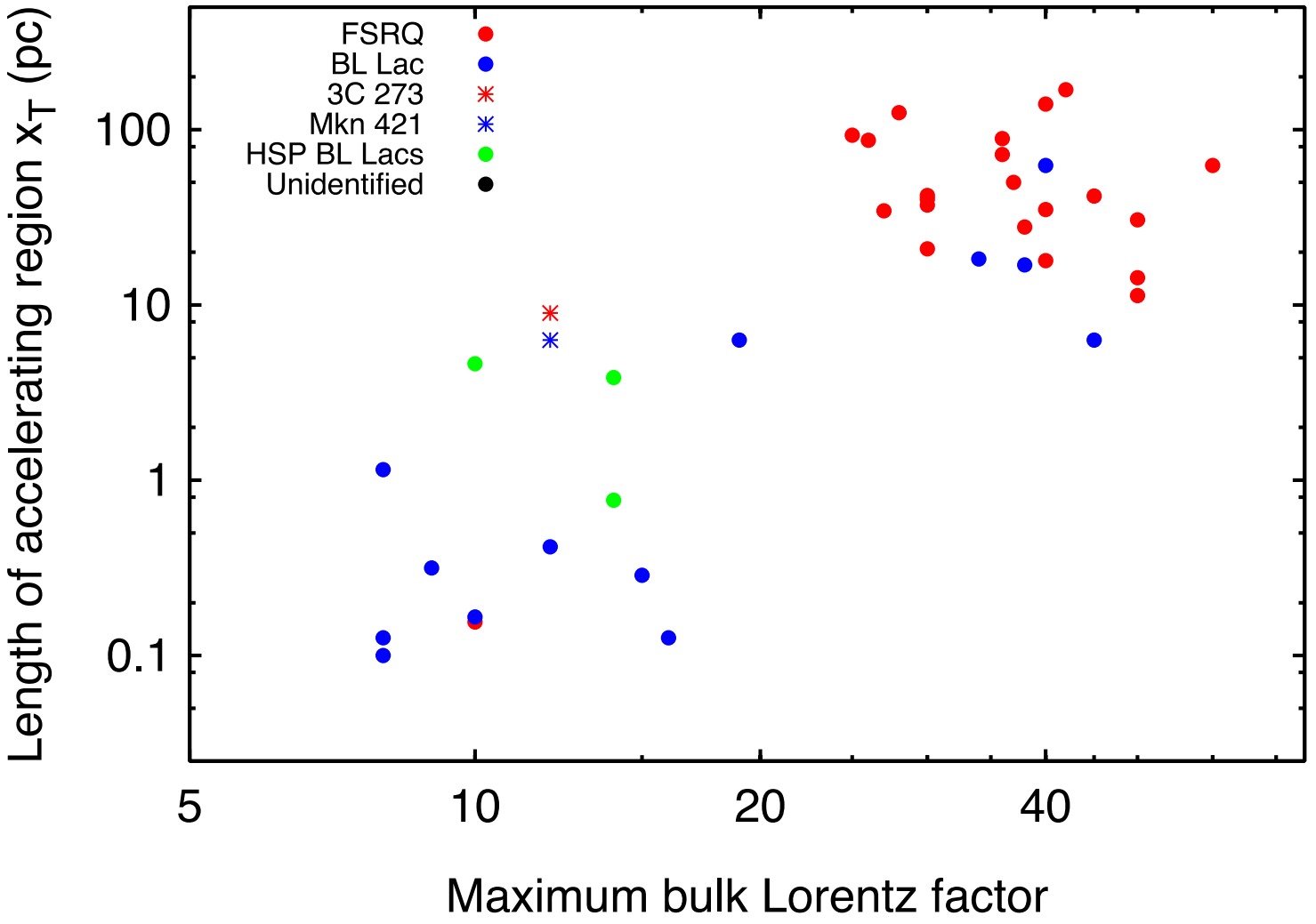

$$\gamma_{bulk} \propto x_T^{1/4}$$

Potter and Cotter 2015

The physics behind the blazar sequence

- Low power BL Lacs have high magnetic field strengths at the transition region so high peak frequency synchrotron emission and SSC.

$$B^2 \propto \frac{Jet\ power}{Radius^2} \propto \frac{1}{Jet\ power}$$

$$Radius \propto Jet\ power$$

- High power FSRQs have lower B fields at transition region so lower peak frequencies.
- FSRQs have larger bulk Lorentz factors so Compton dominance is due to scattering external CMB and NLR photons outside the BLR and dusty torus.

Evidence for an accretion mode dichotomy

- Assuming a fiducial mass MBH=5x$10^8 M_{Sun}$ for all FSRQs and BL Lacs (Shaw et al. 2013).
- The distance in r_s at which the jet comes into equipartition is much larger in FSRQs than BL Lacs.
- The Eddington accretion rate is much lower in BL Lacs than FSRQs.

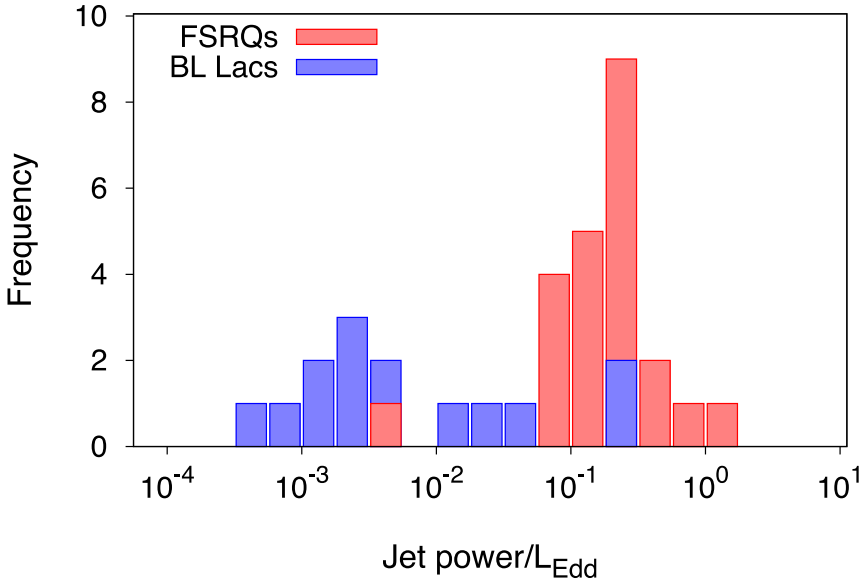

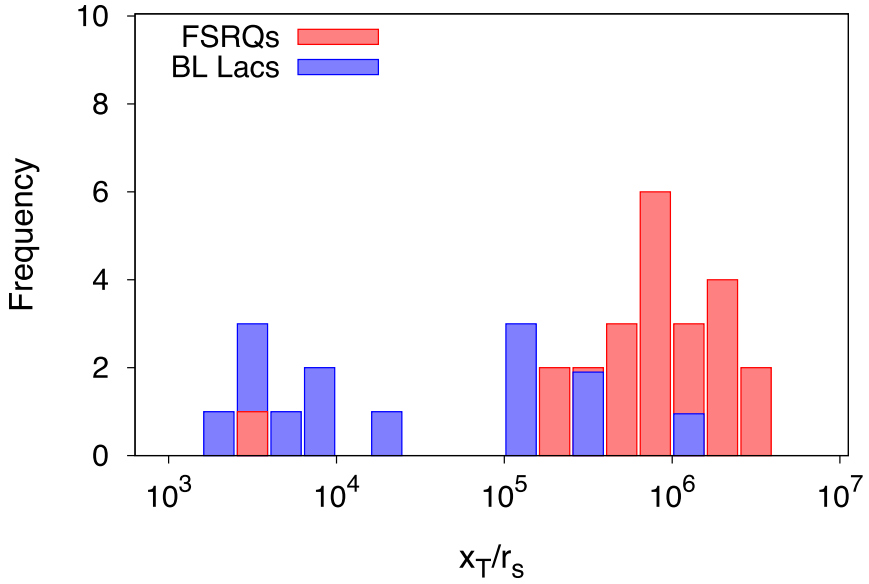

P+C 2015

Evidence for AGN unification

- Similar Eddington distribution to AGN observations of radiatively inefficient Low Excitation Radio Galaxies and radiatively efficient High Excitation Radio Galaxies.

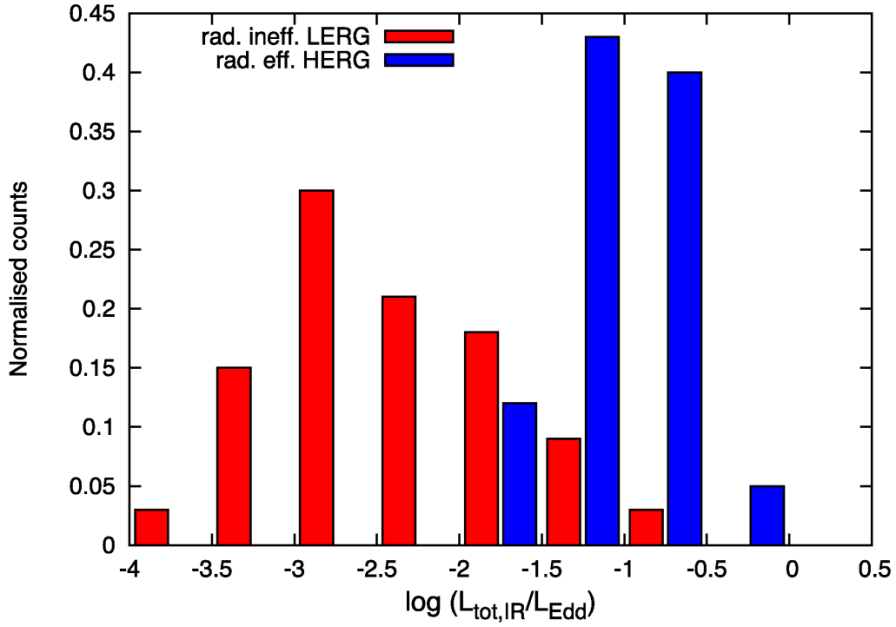

Mingo et al. 2014

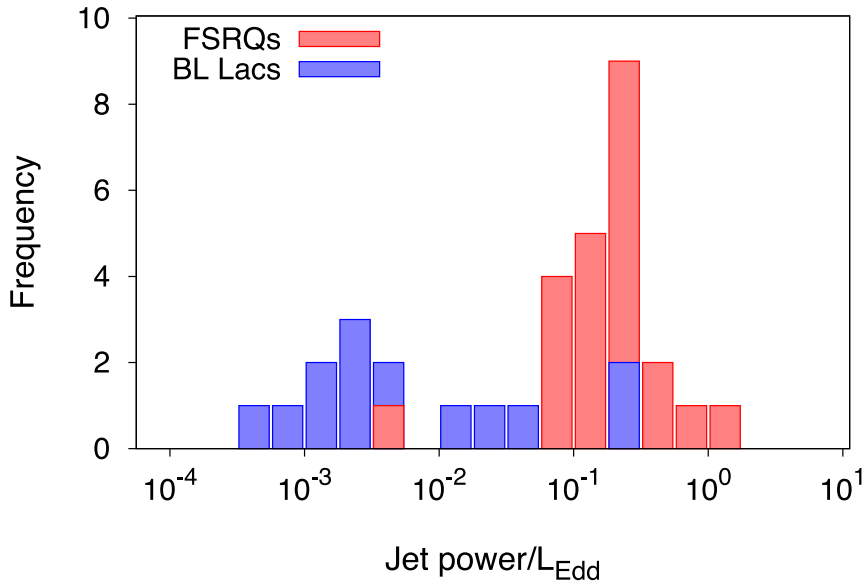

P+C 2015

Conclusions

- Blazar spectra are fitted with unprecedented precision by a realistic fluid jet model with a parabolic accelerating base transitioning to a conical jet at equipartition.
- The radius of the jet at equipartition appears to scale linearly with jet power.
- The jet speed increases with the length of the accelerating base.
- Evidence for a bimodal accretion rate and correspondence between BL Lacs and Lergs (FRIs) and FSRQs and Hergs (FRIIs).

BL Lacs (10^{36}-$5x10^{38}$W)

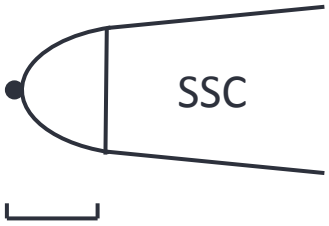

0.1-10pc Γ=5-20

FSRQs ($5x10^{38}$-10^{40}W)

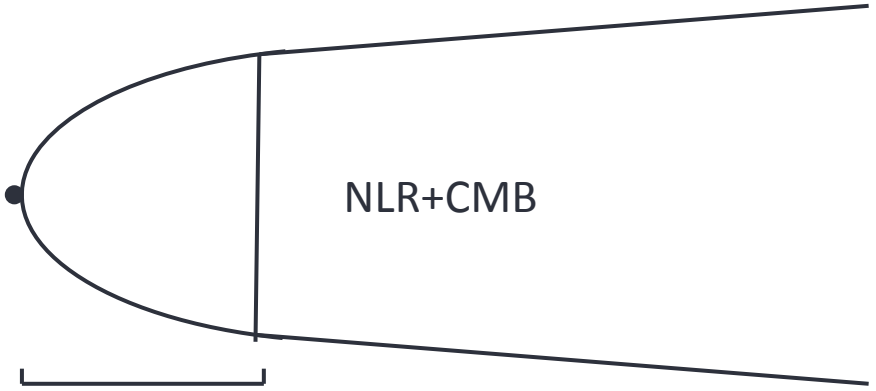

10-100pc Γ>20

Summary

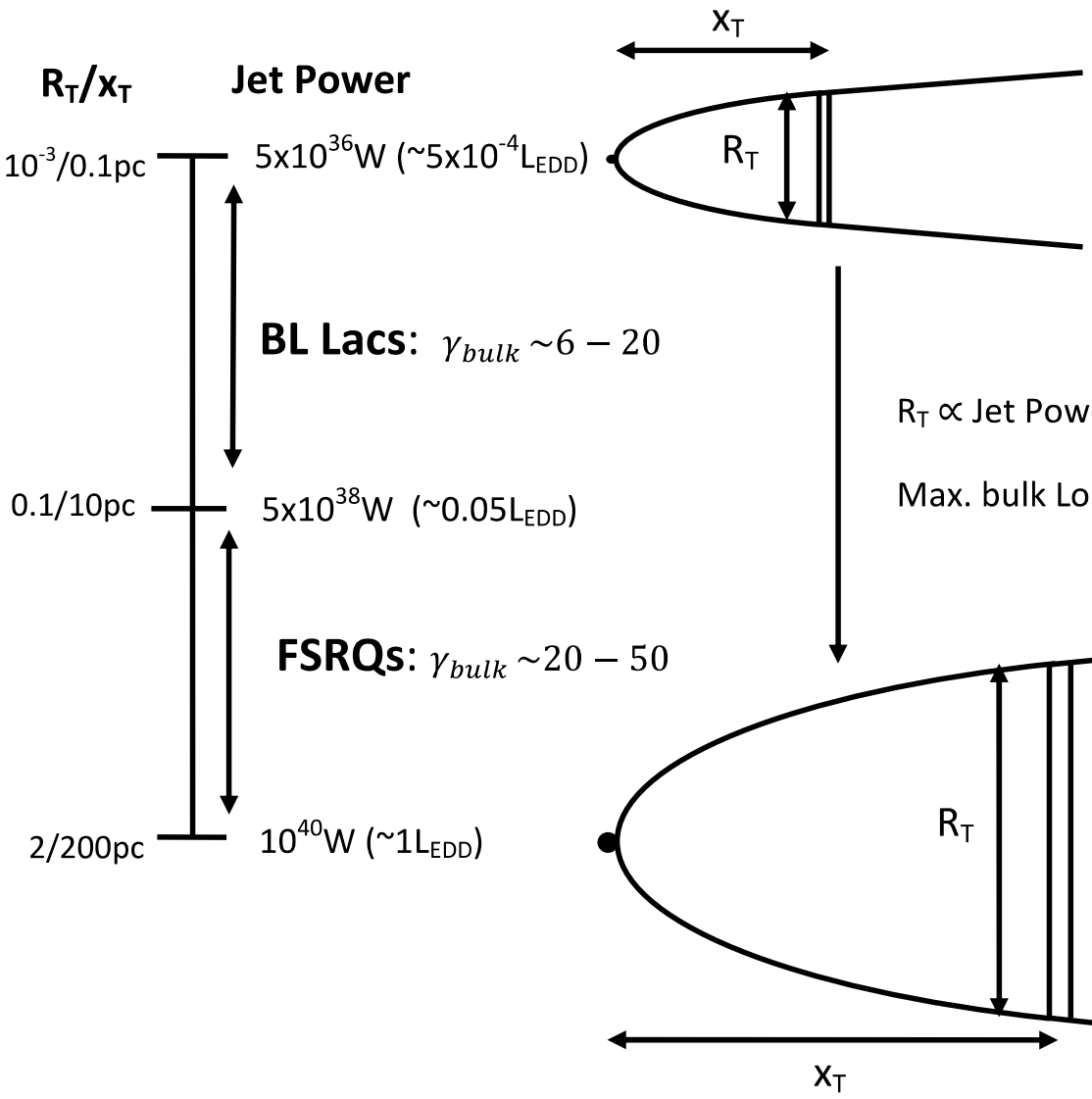

BL Lacs - Small radius transition region with large magnetic field strength leading to high peak synchrotron frequency. Gamma rays dominated by SSC emitted within transition region.

$R_T \propto$ Jet Power

Max. bulk Lorentz factor $\propto R_T^{1/4}$

FSRQs - Large radius transition region with small magnetic field strength leading to low peak synchrotron frequency. Gamma rays dominated by scattering CMB photons at large distances.

A realistic, extended model for jet emission

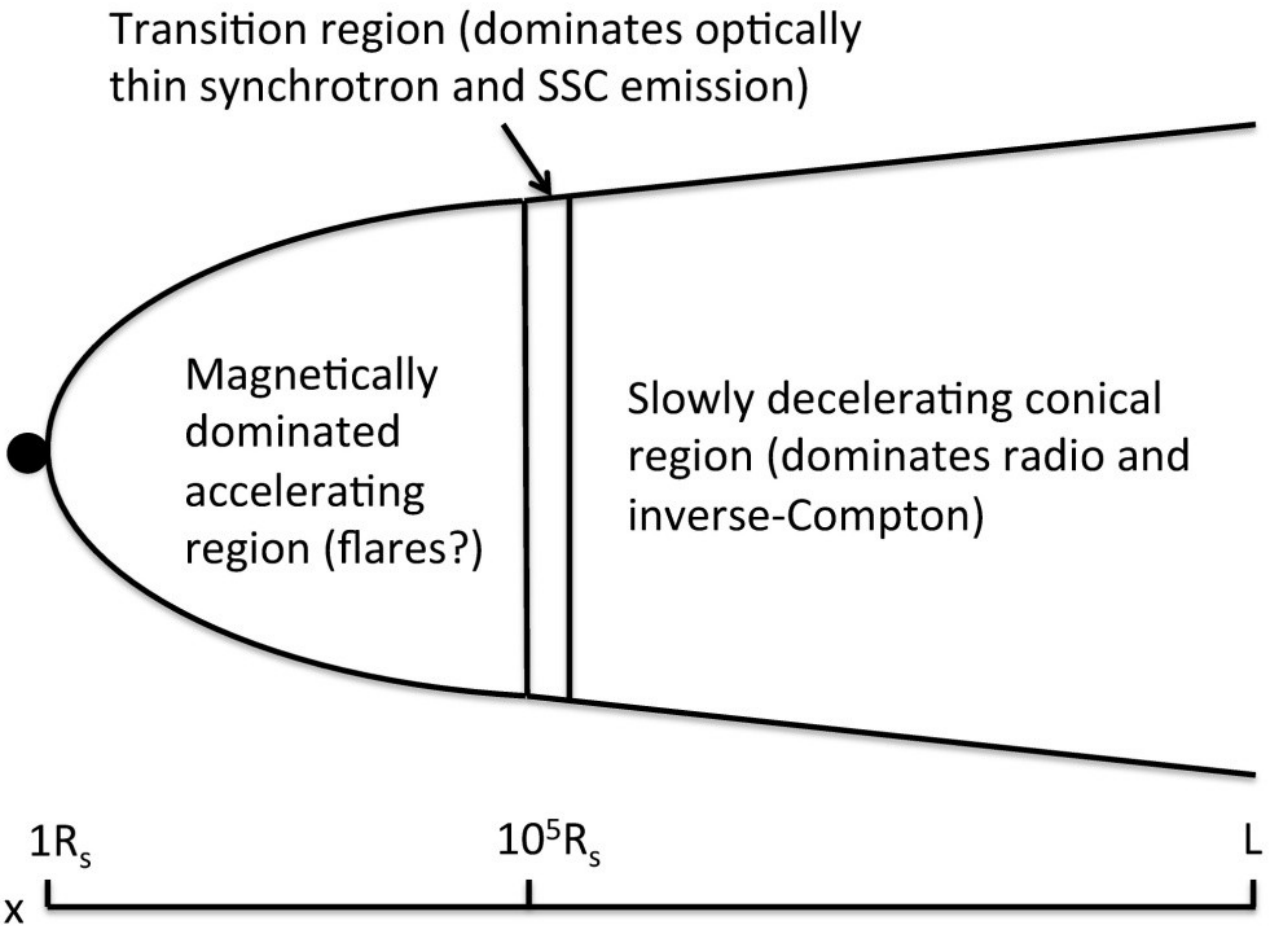

Potter and Cotter 2013a

Particle acceleration

- High energy electrons are required to produce the optical synchrotron emission.
- The process which accelerates these non-thermal electrons is not understood but leading candidates are magnetic reconnection and shock acceleration.
- Since this process is unknown we assume that electrons are injected into the total population with a form:

$$n_e(E_e) \propto E_e^{\alpha} \exp(-E_e / E_{\max})$$

- The radiative energy losses are then taken into account to modify this electron energy spectrum along the jet.
- We conserve the particle flux along the jet.

Physical interpretation

- High power jets are able to accelerate for larger distances before being disrupted by the external medium.
- This means high power jets accelerate to higher bulk Lorentz factors and have larger radii when they stop accelerating.
- This combination explains the main differences between BL Lac and FSRQ spectra and the blazar sequence due to different magnetic field strengths and bulk Lorentz factors.
- The jet powers we find are consistent with a dichotomy in accretion modes between low power BL Lacs and high power FSRQs and this corresponds closely to bimodal accretion rates found for radiatively efficient and inefficient radio galaxies.
- These results support the idea of magnetic acceleration but introduce constraints on length scales and bulk Lorentz factors.
- This suggests a quantitative difference in FSRQ and BL Lac jets which could also be valid for the FRI and FRII dichotomy.
- Much more detail if I had time...

Results

- The fluid model fits observations across all frequencies with unprecedented accuracy.
- By fitting the radio data, specifically, the frequency where the synchrotron emission goes from optically thick to thin we can tightly constrain the radius of the brightest synchrotron emitting region.
- In FSRQs this places the bright transition region at 10-200pc, making it outside the BLR and dusty torus.
- At these large distances the inverse-Compton emission is produced by scattering CMB photons if the jets have high bulk Lorentz factors.
- The transition region of BL Lacs occurs at smaller distances with larger magnetic field strengths.
- BL Lacs have higher peak frequency emission and produce enough synchrotron photons to inverse-Compton scatter.

Acceleration, deceleration and Jet geometry

- Using relativistic conservation laws ensures that when the jet accelerates magnetic energy is converted into bulk kinetic energy.
- In the slowly decelerating conical section the bulk kinetic energy is converted back into internal energy (in situ particle acceleration and enhancement of magnetic field).

Jet Formation and Propagation in FSRQs and BL Lacs

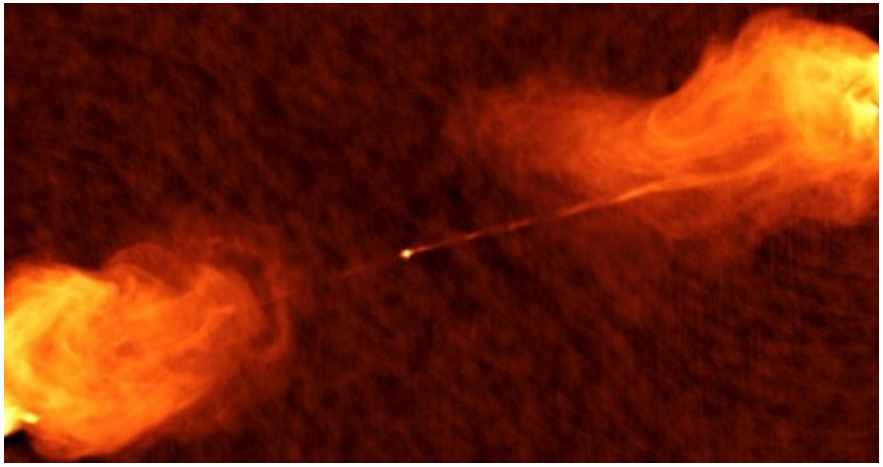

vs.

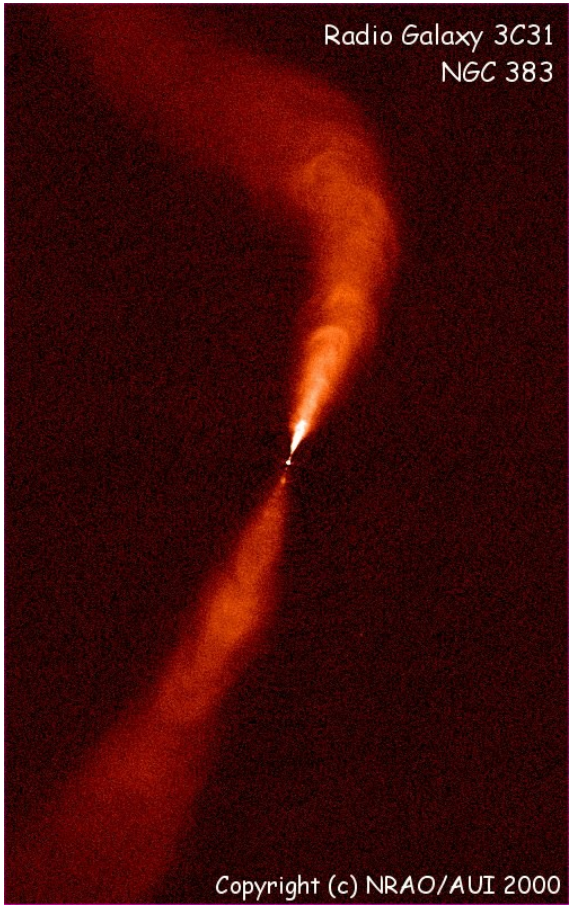

?

William Potter

Junior Research Fellow at University College, University of Oxford

Purpose of my research

- To create the first extended fluid jet model calculating the observed emission which combines prescient observations and theoretical ideas to bridge the gap between simulations and observations.
- To use this to constrain the basic structural and dynamical properties of jets (like the speed and shape) by comparing fluid jet models to observed spectra.
- To understand how systematic differences in spectral properties and classes within the blazar population arise from physical differences.
- Existing models of blazar emission use only one or two spherical blobs and so do not constrain the extended structure or dynamics.

Fluid equations

- There are two main conservation laws: conservation of energy-momentum and conservation of particle number.

$$\nabla_\mu T^{\mu\nu} = 0 \qquad T^{\mu\nu} = T^{\mu\nu}{}_{Magnetic} + T^{\mu\nu}{}_{Particle} + T^{\mu\nu}{}_{EnergyLosses}$$

- Assume a plasma which is homogeneous and isotropic in the rest frame across a slice at constant distance. Assume a time-independent jet.
- The energy momentum tensor is a relativistic perfect fluid.

$$T^{\mu\nu} = diag(\rho, p, p, p) \qquad p = \frac{\rho}{3}$$

$$T^{00}{}_{Magnetic} = \frac{B^2}{2\mu_0} \qquad T^{00}{}_{Particle} = \int_{E\min}^{E\max} n_e(E_e) E_e dE_e$$

$$T^{00}{}_{EnergyLosses} = \frac{\int P_{Synch}(x) + P_{IC}(x) + P_{Adiabatic}(x) dx}{\pi R^2(x)}$$

Converting from the rest frame to lab frame

- Given a homogeneous isotropic perfect fluid in the rest frame the lab frame energy-momentum tensor will be

Rest frame

$$T'^{\mu\nu} = \begin{pmatrix} \rho & 0 & 0 & 0 \\ 0 & \frac{\rho}{3} & 0 & 0 \\ 0 & 0 & \frac{\rho}{3} & 0 \\ 0 & 0 & 0 & \frac{\rho}{3} \end{pmatrix}$$

$$\Lambda^{\mu}{}_{\nu} = \begin{pmatrix} \gamma & \gamma\beta & 0 & 0 \\ \gamma\beta & \gamma & 0 & 0 \\ 0 & 0 & 1 & 0 \\ 0 & 0 & 0 & 1 \end{pmatrix}$$

$$T^{\mu\nu}(x) = \Lambda^{\mu}{}_{a} T'^{ab} \Lambda^{\nu}{}_{b} = \begin{pmatrix} \frac{4}{3}\gamma_{\text{bulk}}(x)^2\rho & \frac{4}{3}\gamma_{\text{bulk}}(x)^2\rho & 0 & 0 \\ \frac{4}{3}\gamma_{\text{bulk}}(x)^2\rho & \frac{4}{3}\gamma_{\text{bulk}}(x)^2\rho & 0 & 0 \\ 0 & 0 & \frac{\rho}{3} & 0 \\ 0 & 0 & 0 & \frac{\rho}{3} \end{pmatrix}$$

Lab frame

Conservation of energy

$$\int \nabla_\mu T^{\mu\nu} d^4V = \oint T^{\mu\nu} d^3S_\mu = 0$$

$$= \int_0^R \int_x^{x+dx} \int_0^{2\pi} T^{t\nu} R d\theta dx dR + \int_t^{t+dt} \int_0^{dR} \int_0^{2\pi} T^{x\nu} R d\theta dR dt + \ldots$$

$$+ \int_t^{t+dt} \int_0^{x} \int_0^{2\pi} T^{R\nu} R d\theta dx dt + \int_t^{t+dt} \int_0^{dR} \int_0^{x} T^{\theta\nu} R dx dR dt$$

No time dependence so =0

$$= \left[\pi R^2 T^{t\nu} \right]_x^{x+dx} = \frac{\partial}{\partial x} \left(\pi R^2 \frac{4\gamma^2 \rho_{rest}}{3} \right) dx = 0$$

Synchrotron and inverse-Compton emission

- To calculate the synchrotron and inverse-Compton emission we transform into the local rest frame.

$$P_{Synch} = \frac{4}{3}\sigma_T c\beta^2\gamma^2 U_B \qquad P_{IC} = \frac{4}{3}\sigma_T c\beta^2\gamma^2 U_{radiation}$$

- External photon fields are Doppler-boosted in the rest frame and we use the full Klein-Nishina cross section.
- We include all relevant photon sources as a function of distance.
- We integrate the optical depth due to synchrotron self-absorption and pair production along the jet.

Conservation of particle flux

$$\nabla_\mu J^\mu = 0 \qquad J^\mu = n_e U^\mu = n_e \gamma (c, v, 0, 0)$$

- Again using the divergence theorem and time-independence as before we arrive at the continuity equation.

$$\frac{\partial}{\partial x}\left(\pi R^2 J^t\right) dx = \frac{\partial}{\partial x}\left(\pi R^2 n_e \gamma c\right) = 0$$

Length contraction

- So the rest frame particle energy density goes as gamma^{-1}, magnetic energy as gamma^{-2}.
- Jets become more particle dominated as they accelerate.

Emission from different components

- Flat spectrum from different sections of conical jet.
- Inverse-Compton from CMB for FSRQs SSC for BL Lacs.

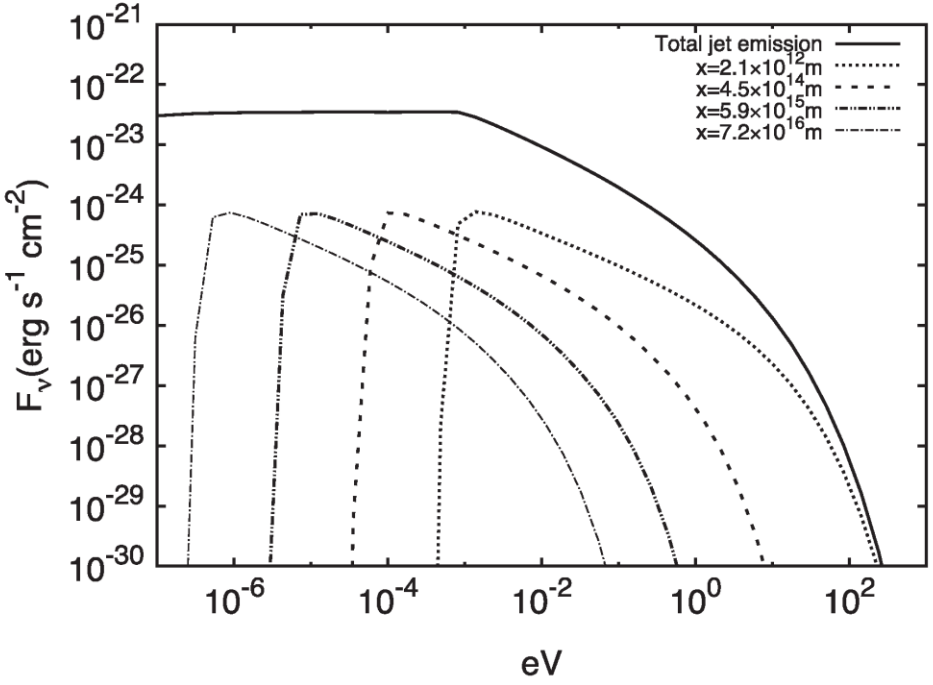

P+C 2012

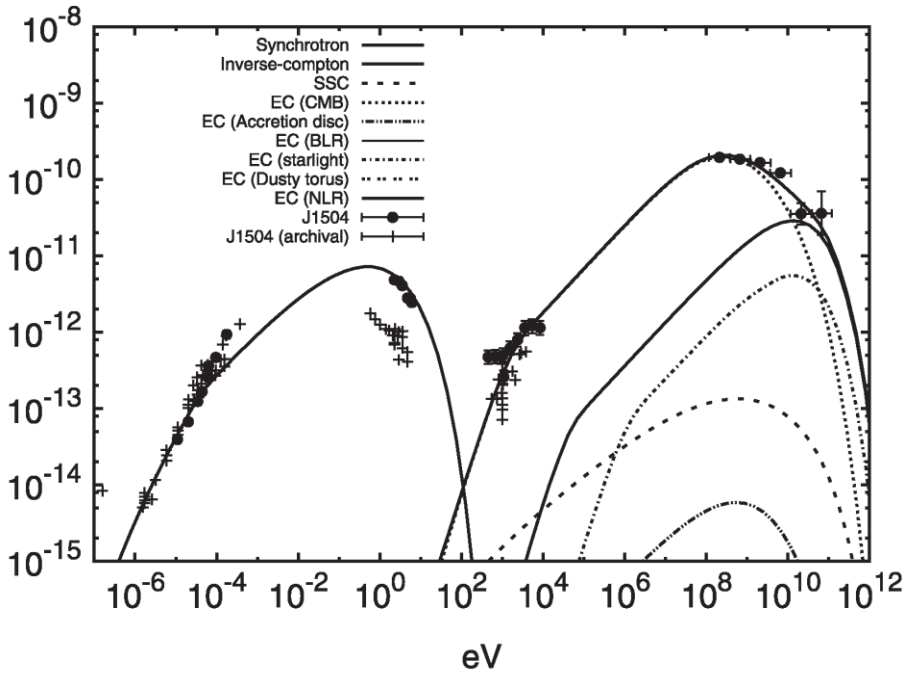

P+C 2013b

Model Assumptions

- Our model incorporates the latest results from theory, simulations and observations.
- The jet has a geometry set by the observations of M87 and scaled linearly.
- The jet starts with an accelerating magnetically dominated parabolic region with an acceleration profile consistent with simulations and theory.
- It accelerates up to the transition region where the acceleration ceases to be efficient, non-thermal particle acceleration occurs and the jet first comes into equipartition.
- After the bright transition region the jet remains close to equipartition in the slowly decelerating conical section.
- This is the first emission model to include acceleration and deceleration and to have a variable shape.

Accretion discs and jets

- If a black hole is surrounded by gas it forms an accretion disc and sometimes a jet.
- More detail later...

Model assumptions

- Although the code is completely flexible we need to make some simplifying assumptions to constrain the parameters.
- The jet is magnetically dominated up to the transition region.
- At the transition region the jet comes into equipartition between non-thermal electrons and magnetic energies.
- The conical section is observed to be close to equipartition between magnetic and non-thermal electron energies (Croston et al. 2005 + Homan et al. 2006).

Observations and simulations of jets

- VLBI observations of M87 show the jet starts with a parabolic shape and this transitions to conical at $10^5 r_s$ (Asada and Nakamura 2011).
- Simulations show a jet which starts magnetically dominated and parabolic (Mckinney et al. 2006...).
- The jet stops accelerating at equipartition and tends to become ballistic and conical (Komissarov et al. 2009).
- MHD simulations are computationally intensive so radiation processes are ignored, we need an emission model which can compare jet structure and dynamics to observations of jets.